

1 Aerosol optical properties derived from POLDER- 2 3/PARASOL (2005-2013) over the western Mediterranean Sea 3 – Part 2 : Spatial distribution and temporal variability

4
5 Isabelle Chiapello¹, Paola Formenti², Lydie Mbemba Kabuiku², Fabrice Ducos¹, Didier
6 Tanré¹, François Dulac³

7
8 ¹Univ. Lille, CNRS, UMR 8518 – LOA – Laboratoire d’Optique Atmosphérique, F-59000 Lille, France

9 ²LISA, CNRS UMR 7583, Université Paris Est Créteil, Université de Paris, IPSL, Créteil, France

10 ³LSCE/IPSL, CEA-CNRS-UVSQ, Université Paris-Saclay, Gif-sur-Yvette, France

11
12 *Correspondence to:* Isabelle Chiapello (isabelle.chiapello@univ-lille.fr)

13
14 **Abstract.** The Mediterranean atmosphere is impacted by a variety of natural and anthropogenic aerosols, which
15 exert a complex and variable pressure on the regional climate and air quality.

16 ~~In This study, we investigate aerosol spatial distribution and temporal evolution over~~ focuses on the western
17 Mediterranean Sea (west of longitude 20°E) using the full POLDER-3/PARASOL aerosol data record derived
18 from the operational clear-sky ocean algorithm (collection 3) available from March 2005 to October 2013. This
19 8.5-yr satellite data set includes retrievals at 865 nm of the total, fine, and coarse mode aerosol optical depth (AOD,
20 AOD_F, and AOD_C, respectively), Angström exponent (AE), and the spherical/non-spherical partition of the coarse-
21 mode AOD (AOD_{CS} and AOD_{CNS}, respectively), that **have been carefully validated over the study region (Formenti**
22 **et al., 2018).**

23 ~~In a previous paper (Formenti et al., 2018), these POLDER 3 derived aerosol properties have been carefully~~
24 ~~validated over the study region, based on coincident ground based and airborne aerosol measurements.~~

25 Here we analyze the spatial distribution, the seasonal cycle, and interannual variability of this ensemble of
26 **advanced aerosol** products in three latitude bands (34-38°N, 38-42°N, and >42°N) and for three sites (Ersa,
27 Barcelona, Lampedusa) distributed on the western basin.

28 **POLDER-3 retrieves the high influence of north African desert dust over the region, which largely controls the**
29 **spatial distributions (south-to-north decreasing gradient) and seasonal cycles (spring/summer maximum) of both**
30 **AOD and coarse AOD, including its non-spherical component. In contrast, the coarse spherical component of**
31 **AOD remains relatively homogeneously low all year long over the region, whereas fine mode AOD are generally**
32 **more elevated in the eastern part of the region of study, especially north of the Adriatic Sea.**

33 ~~Overall the POLDER 3 AOD spatial distribution exhibits a well known south to north decreasing gradient, and a~~
34 ~~seasonal cycle characterized by enhanced aerosol loads in spring and summer, both controlled by Saharan dust.~~

35 ~~POLDER 3 retrievals of AE, AOD_F, AOD_C, and fine mode fraction (AOD_F/AOD) highlight the influence of coarse~~
36 ~~particles in the southern part of the region, off the north African coast, and higher relative contribution of fine~~
37 ~~particles in the northern part, off the south European coast, with all year long persistent elevated loads over the~~
38 ~~Adriatic Sea. Over the rest of the western Mediterranean Sea, POLDER 3 retrievals show a more homogeneous~~
39 ~~spatial distribution of fine particles than that of coarse particles, even though climatological means of AOD_F~~
40 ~~highlight seasonal differences in the order of a factor 2 between the cleanest conditions occurring in the southern~~
41 ~~part of the basin in winter and those most polluted observed in its northern part in Spring. The seasonal and spatial~~

42 variability of AOD_{CNS} is close to that observed for AOD_C, whereas POLDER-3 exhibit relatively low and weakly
43 variable levels of coarse spherical particles (AOD_{CS} < 0.05).

44 ~~Over the whole 2005-2013 period~~ From 2005 to 2013, annual POLDER-3 AOD evolution shows a decreasing trend
45 (\approx of 0.0030 per year in absolute value at 865 nm (0.060 per year at 550 nm). Such a downward evolution ~~decrease~~
46 is much more pronounced and spatially extended for AOD_F (- 0.0020 per year at 865 nm) than for AOD_C (~~\leq 0.002~~
47 ~~per year~~). Our analysis also suggests that the North Atlantic Oscillation (NAO) index explains a significant part
48 of the interannual variability of POLDER-3 AOD_C, reflecting its role on the frequency of Saharan dust transport
49 over the region. Finally, the POLDER-3 dataset highlights an improvement of air quality related to the fine aerosol
50 component, with a marked evolution toward more frequent occurrence of clean conditions (\geq 75 70% of daily
51 AOD_{F-865 nm} < 0.05) at the end of the period of study (2010-2013) over most of the western Mediterranean Sea,
52 and much less evidence of such a large-scale evolution for the coarse mode fraction. Therefore, despite the high
53 and variable influence of mostly natural north African dust over the region, the POLDER-3 advanced aerosol
54 dataset appears sufficiently accurate to successfully resolve the concurrent downward trend of fine, primarily
55 anthropogenic particles, most likely related to reduced emissions in the surrounding European countries.

56

57 1 Introduction

58

59 Due to the contributions of diverse natural and anthropogenic sources and because of their relatively short lifetime
60 in the troposphere, aerosols consist in a complex, timely and spatially variable mixture of particles (Boucher,
61 2015). As aerosol impacts, especially in terms of air quality degradation and radiative forcing contribution to
62 climate change, strongly depend on both very variable aerosol loads and properties, they require a dedicated
63 reliable monitoring. Despite a number of measurements efforts deployed in the last decades (Laj et al., 2009;
64 Pandolfi et al., 2018; Formenti, 2020; Laj et al., 2020), the variety of atmospheric particles, in terms of loads, size
65 ranges, shapes, chemical compositions, and optical properties remains partially characterized. Indeed, the
66 monitoring of the spatial, temporal, and vertical variability of all these physico-chemical parameters in both an
67 accurate and comprehensive way is still a challenge. Significant advances have been achieved by intensive field
68 experiments deploying detailed but limited in time and space *in situ* measurements of aerosol chemical, physical,
69 and optical properties (e.g. Denjean et al., 2016; Di Biagio et al., 2016). In parallel, remote sensing observations,
70 especially those from ground-based global aerosol networks, like AERONET (Holben et al., 2001), and dedicated
71 advanced aerosol satellite sensors, like MODIS (MODerate resolution Imaging Spectrometer) or POLDER
72 (POLarization and Directionality of the Earth's Reflectances) (Tanré et al., 2011; Bréon et al., 2011; Remer et al.,
73 2020), have made considerable progress in expanding in time and space the aerosol datasets acquired from field-
74 experiments. Thus, remote sensing has become an essential complementary tool, able to provide unique repetitive
75 and large-scale view of aerosol loads and properties evolution. The combination of both types of measurements,
76 i.e. detailed *in situ* aerosol characterization and long-term repetitive aerosol properties monitored by space-borne
77 sensors is required to improve current understanding of their evolution in terms of loads and properties and to
78 reduce uncertainties on their impacts.

79 This paper is dedicated to a regional aerosol analysis based on retrievals from POLDER-3/PARASOL
80 (Polarization & Anisotropy of Reflectances for Atmospheric Sciences coupled with Observations from a Lidar)
81 satellite sensor over the period 2005-2013 in the western Mediterranean Sea. This region, impacted by
82 demographic pressure and air quality degradation, is under the influence of both anthropogenic and natural

83 aerosols, emitted from different types of continental and marine sources (e.g. Lelieveld et al., 2002; Di Biagio et
84 al., 2015; Ancellet et al., 2016; Chazette et al., 2016, Claeys et al., 2017; Michoud et al., 2017; Chazette et al.,
85 2019). Therefore, in the recent years, it has experienced an increasing scientific interest as shown by a number of
86 studies dedicated to Mediterranean aerosol characterization through large-scale field-experiments (e.g., Di Biagio
87 et al., 2015; Mallet et al., 2016; Ricaud et al., 2018 and references therein), modeling efforts (Rea et al., 2015;
88 Menut et al., 2016, Sič et al., 2016; Chrit et al., 2018; Drugé et al., 2019), and satellite observations analysis (Nabat
89 et al., 2013; Floutsi et al., 2016).

90 ~~Historical long-term aerosol satellite datasets have been used to investigate the influence and evolution of north~~
91 ~~African mineral dust transported over this region (Dulac et al., 1992; Moulin et al., 1998; Antoine and Nobileau~~
92 ~~2006; Gkikas et al., 2013, 2016).~~

93 Previous studies relying on daily, large-scale satellite aerosol observations (Dulac et al., 1992; Moulin et al., 1998;
94 Antoine and Nobileau 2006; Gkikas et al., 2013, 2016) have highlighted that the Mediterranean atmosphere is
95 highly influenced by the sporadic transport of north African dust. This export causes a south to north decreasing
96 gradient of aerosol loads, and a seasonal east-west shift characterized by a later (summer) maximum for the western
97 basin (Moulin et al., 1998; Floutsi et al., 2016). In addition, several long-term satellite data sets have revealed the
98 large-scale control of the North Atlantic Oscillation on the inter-annual variability of retrieved aerosol loads, in
99 relation to this highly variable transport of dust over the region (Moulin et al., 1998; Antoine et Nobileau, 2006).

100 Floutsi et al., (2016) climatology, based on 12 years of MODIS aerosol observations (2002-2014), has highlighted
101 a decreasing trend of aerosol loads over the Mediterranean basin. Their MODIS data set, by showing a higher
102 decreasing trend of fine-mode aerosol loads than that of the coarse fraction, strongly suggests a lowering of
103 anthropogenic pollution particles influence over the region, most likely related to reduced human-related
104 emissions. In agreement with other multiyear satellite studies (Gkikas et al., 2013), Floutsi et al. (2016) also assume
105 a certain level of decrease of the transported desert dust particles, mainly over the western sub-basin.

106 Most of the satellite studies dedicated to interpretation of aerosol spatial and temporal variability over the
107 Mediterranean region have been relying on MODIS retrievals (Barnaba and Gobi, 2004; Hatzianastassiou et al.,
108 2009; Georgoulas et al., 2016), with some of them focusing of the eastern sub-basin (Georgoulas et al., 2016;
109 Shaheen et al., 2020). Considering the complexity of the aerosol influences in the Mediterranean atmosphere and
110 inherent uncertainties related to long-term satellite aerosol retrievals, our study aims to provide a first interpretation
111 of an independent advanced aerosol satellite data set. For this purpose, we investigate the POLDER-3/PARASOL
112 data set (Herman et al., 2005; Tanré et al., 2011), which offers the capacity for daily monitoring of the size-resolved
113 aerosol properties over sea surfaces over its almost 9 years period of operation (Formenti et al., 2018).

114 At a global scale, a careful validation of POLDER-3 aerosol retrievals ~~validation~~ has been performed for derived
115 total and fine aerosol optical depth (AOD), through statistical comparison to ~~coincident~~ sun/sky photometer data
116 of the AERONET network ~~at a global scale~~ (Bréon et al., 2011). In a first dedicated paper (part 1 of the present
117 paper: Formenti et al., 2018), we lead a regional comprehensive quality assessment of POLDER-3 derived aerosol
118 parameters over the western Mediterranean Sea, based on both aerosol measurements from 17 ground-based
119 coastal and insular AERONET sites over the period 2005-2013, and in situ airborne observations available during
120 summer 2012 and 2013 Chemistry-Aerosol Mediterranean Experiment (ChArMEx) experiments (Di Biagio et al.,
121 2015; Mallet et al., 2016). Our analysis has highlighted quality and robustness of POLDER-3 operational aerosol
122 retrievals over oceans, especially total, fine, and coarse AOD (AOD, AOD_F, and AOD_C) at 865 nm, Angström

123 Exponent (AE), and the spherical and non-spherical partition of coarse-mode AOD (AOD_{CS} and AOD_{CNS}) over
124 this region. In this paper, the advanced aerosol data set provided by POLDER-3 over its operating period, i.e. from
125 March 2005 to October 2013, is investigated in terms of spatial variability and temporal evolution of aerosol load,
126 **size, and shape** properties over the western Mediterranean Sea.

~~127 Specific studies, often based on MODIS aerosol retrievals or combining MODIS to other complementary aerosol
128 satellite data sets, have attempted to separate the contributions of different aerosol types prevailing in the
129 Mediterranean region, i.e. maritime aerosols, continental/anthropogenic aerosols, and African dust (Barnaba and
130 Gobi, 2004; Hatzianastassiou et al., 2009; Georgoulas et al., 2016). Despite the increasing number of satellite-
131 based aerosol studies, especially in the East part of the Mediterranean area (Georgoulas et al., 2016; Shaheen et
132 al., 2020), it is noticeable that no investigation of POLDER 3/PARASOL aerosol products (Herman et al., 2005;
133 Tanré et al., 2011) has been performed yet over this region, despite its potential for monitoring the size resolved
134 aerosol properties over sea surfaces over its almost 9 years period of operation (Formenti et al., 2018).~~

~~135
136 In order to ensure a reliable regional view of aerosol loads and properties evolution from satellites, aerosol
137 retrievals derived from different sensors and algorithms require careful evaluation.~~

138

139 **2 POLDER-3 instrument and derived aerosol operational products over ocean**

140
141 POLDER-3 (POLarization and Directionality of the Earth's Reflectances) instrument on board the PARASOL
142 (Polarization & Anisotropy of Reflectances for Atmospheric Sciences coupled with Observations from a Lidar)
143 mission is dedicated to advanced aerosol monitoring (Tanré et al., 2011). PARASOL, launched in December 2004
144 in order to be part of the A-Train, has been in operation from March 4, 2005 to October 10, 2013. Over this period,
145 data availability is 91%. The explanations for the 9% loss of data are multiple: orbital maneuvers, instrument put
146 on standby for security reasons, data transmission between the payload and the receiving station, and problems
147 encountered with the stellar sensor. POLDER-3 payload consisted of a digital camera with a 274 x 242 –pixel
148 CDD detector array, wide-field telecentric optics and a rotating filter wheel enabling measurements in 9 spectral
149 channels from blue (443 nm) to near-infrared (1020 nm). Polarization measurements were performed at 490 nm,
150 670 nm, and 865 nm. With an acquisition of a sequence of images every 20 sec, the instrument could observe
151 ground targets from up to 16 different angles, +/-51° along track and +/-43° across track (Tanré et al., 2011). The
152 original pixel size is 5.3 km x 6.2 km at nadir. Algorithms have been developed to process the POLDER
153 measurements in order to retrieve aerosol parameters at 18.5 x 18.5 km² superpixel resolution (3 x 3 pixels). In
154 this paper, we use the operational clear-sky ocean retrieval algorithm (Herman et al., 2005) derived from collection
155 3, corresponding to the latest update performed in 2014 that included calibration improvements (Fougnie, 2016).
156 This algorithm, described in details by Herman et al. (2005) and Tanré et al. (2011), has been slightly improved in
157 collection 3 regarding non-spherical particles in the coarse mode (Formenti et al., 2018). Briefly, it is based on the
158 total and polarized radiances measured at 670 and 865 nm. Using a look up table (LUT) built on aerosol
159 microphysical models (described in Table S1 in the Supplement of Formenti et al., 2018), the algorithm
160 recalculates for each clear sky pixel the observed polarized radiances at several observational angles. Importantly,
161 in the aerosol models used for the inversion, aerosols are considered as non-absorbing (the imaginary part of the
162 refractive index is assumed as zero) and the real part of their refractive index is invariant between 670 and 865
163 nm. The aerosol number size distribution is lognormal and bimodal with an effective diameter smaller (larger)

164 than 1.0 μm for the fine (coarse) mode. The coarse mode includes a non-spherical fraction based on the spheroidal
165 model from Dubovik et al. (2006), whereas a Mie model for homogeneous spherical particles is used to calculate
166 multi-spectral and multi-angle polarized radiances. As an improvement compared to former versions of the
167 algorithm, the effective diameter of the spheroidal model is allowed to take two values (namely 2.96 and 4.92 μm)
168 in collection 3 (Table S1 of Formenti et al, 2018). Within the coarse mode, the non-spherical fraction is set to 5
169 discrete values (0.00, 0.25, 0.50, 0.75, and 1.00, Tanré et al. (2011)). A quality flag index (0 indicating the lowest
170 and 1 the highest quality) is attributed to each superpixel depending on the inversion quality. As in Formenti et al.
171 (2018), only POLDER-3 aerosol products derived from pixels with a quality flag ≥ 0.5 have been considered in
172 our analysis. In the present study, we focus on the western Mediterranean region, west of longitude 20°E,
173 considering the main aerosol parameters derived by POLDER-3 ocean operational algorithm: (i) available for all
174 clear sky pixels: total, fine, and coarse aerosol optical depth (respectively AOD, AOD_F, and AOD_C) at 865 nm,
175 and Angström Exponent between 670 and 865 nm (AE), (ii) available only when the geometrical conditions are
176 optimal (scattering angle range of roughly 90°-160°): spherical and non-spherical fractions of the AOD in the
177 coarse mode (f_{CS} and f_{CNS} respectively), allowing to assess AOD_{CS} and AOD_{CNS} (spherical and non-spherical
178 coarse AOD, respectively) at 865 nm. The quality of these POLDER-3 derived aerosol parameters has been
179 evaluated over the region of interest by Formenti et al. (2018), using co-located in situ airborne measurements
180 from summer 2012 and 2013 field-experiments and coincident ground-based AERONET data available from 17
181 insular and coastal sites over the whole POLDER-3 operation period (2005-2013). This first comprehensive
182 regional evaluation has provided new assessments of uncertainties and highlighted the good quality of collection
183 3 POLDER-3 aerosol data set over our area of interest (Table 4 of Formenti et al., 2018). In our regional analysis
184 of spatial distribution and temporal variability of POLDER-3 aerosol retrievals, the AOD, AOD_F, and AOD_C
185 derived at 865 nm will be complemented, through an extrapolation with the Angström Exponent, by those at 550
186 nm, which is the standard wavelength of many aerosol satellite retrievals and model simulations (Nabat et al.,
187 2013).

188 **3 Results**

189 **3.1 Mean regional and seasonal picture (2005-2013)**

192 The climatological (March 2005 – October 2013) seasonal maps of POLDER-3 derived AOD, AE, AOD_F, AOD_C,
193 AOD_F/AOD (i.e. Fine Mode Fraction or FMF), AOD_{CNS}, and AOD_{CS} at 865 nm over marine areas in the region
194 30-50°N, 10°W-20°E, i.e. mainly the western Mediterranean Sea, are shown in Figure 1. The total AOD (left
195 panels) exhibits a pronounced seasonality with minimum values in winter (defined by the December-January-
196 February months): AOD < 0.10 over most of the region of study. In spring (March-April-May), AOD shows an
197 increase, especially intense over the southeastern part of the region between Italy and Africa, whereas the
198 maximum AOD values (≥ 0.20) are reached in summer (June-July-August) over the whole southern part of the
199 area. In autumn (September-October-November), the AOD over the region are mostly low, comparable to winter
200 loads, except over the southeastern part of the domain, especially over the Ionian Sea, and off the coast of Tunisia,
201 Lybia and south of Sicily, where they reach moderate values (range 0.10 – 0.15). This area of enhanced aerosol
202 transport is geographically similar to that associated to maximum AOD (~ 0.20) in spring. In general, the seasonal
203 POLDER-3 total AOD maps exhibit a well-established south-to-north gradient, with a decrease of values toward
204 the northern part, reflecting the high influence of aerosol sources from the North African continent. This aerosol

205 spatial distribution is consistent with that derived by other satellite sensors over the Mediterranean basin (for
206 example Moulin et al., 1998, Barnaba and Gobi, 2004; Papadimas et al., 2008). The $AE_{865-670\text{ nm}}$ seasonal maps
207 (second column panels) highlight the influence of coarse aerosols (associated with low AE values) in the south
208 part of the region off the north African coast, and higher contribution of fine particles along the coasts of Europe,
209 especially over the Adriatic Sea, where AE values are equal or higher than 1, in all seasons. AOD_F , AOD_C , and
210 AOD_F/AOD (FMF) seasonal maps, shown in the three central column panels, confirm this pattern of spatial
211 variability, typical of coarse and fine aerosol repartition in the Mediterranean basin. The seasonal and spatial
212 variability of AOD_{CNS} is close to that observed for AOD_C , whereas POLDER-3 retrievals of AOD_{CS} suggest a
213 relatively homogeneous repartition of coarse spherical particles, with low values ($AOD_{CS} < 0.05$), and no
214 substantial spatial and seasonal variations (right panels of Figure 1). Figure S1 of the supplementary material
215 complements these POLDER-3 seasonal maps at 865 nm, with AOD , AOD_F , AOD_C , and AOD_F/AOD (i.e. FMF)
216 extrapolated at 550 nm. At this wavelength, AOD reach higher values (≥ 0.30 during summer maximum), **in**
217 **agreement with $AOD_{550\text{ nm}}$ range of retrievals from reference satellite sensors like MODIS and MISR over the**
218 **region (Nabat et al., 2013). As expected, POLDER-3 AOD_F are strongly enhanced (values up to 0.16-0.20)**
219 **compared to 865 nm (< 0.08), whereas AOD_C values are only slightly modified. These ranges of values are**
220 **consistent with the stronger wavelength dependence of AOD of small particles, characterized by high AE values,**
221 **inducing pronounced increase of AOD_F values toward shorter wavelengths. Thus, the spatial distribution of**
222 **POLDER-3 AOD_F at 550 nm is characterized by maximum values (> 0.10) over the eastern part of the region of**
223 **study, and seasonal peaks in spring and summer. North of the Adriatic Sea, POLDER-3 highlights an area**
224 **characterized by all-year persistent high values of AOD_F (> 0.12 at 550 nm), most probably reflecting**
225 **accumulation of pollution particles due to influence of regional anthropogenic sources (as for example from**
226 **Northern Italy in the Po Valley). Such a spatial pattern is fully consistent with the recent analysis of Hansson et**
227 **al. (2021) highlighting that polluted air masses coming from the north along the Adriatic Sea are affecting air**
228 **quality in a large part of the Mediterranean.**

229 230 **3.2 Sub-regional features**

231 In order to examine more deeply the seasonal variations of POLDER-3 aerosol retrievals accounting for the south-
232 to-north gradient observed in Figure 1, the area of study has been divided into three main latitudinal sub-regions.
233 These regions are illustrated in Figure 2. They correspond respectively to the northern part (north of latitude 42°N :
234 zone 1 called NW MED), the central part (latitude band $38 - 42^\circ\text{N}$, zone 2 called CW MED), and the southern
235 part (south of latitude 38°N : zone 3 called SW MED) of the western Mediterranean Sea ($6^\circ\text{W} - 20^\circ\text{E}$).

236 Figure S2 of the supplementary material reports the statistics of the POLDER-3 retrievals over the March 2005-
237 October 2013 time period in each-sub-region, with mean and standard deviations, maximum and minimum values
238 of number of available clear-sky superpixels (left column) and number of available days of observations for each
239 month and year (right column). ~~The maximum number of POLDER-3 superpixels (left panels) is 434 in NW MED~~
241 ~~and up to 1232 in SW MED and 1384 in CW MED, reflecting the smaller size of the NW-MED sub-region.~~ As
242 expected, more POLDER-3 retrievals are available in summer than in winter months, due to the higher influence
243 of cloudiness during the cold season. The number of days with aerosol retrievals by month and year for each sub-
244 region (right column) highlights that more than 50% of daily POLDER-3 retrievals are available for most of the
245 months of the whole time period. A few exceptions occur for some specific months, as July 2007 and July 2010,

246 common at the three sub-regions due to missing data during these periods related to instrumental problems with
247 the solar sensor (only 28% and 14% of data available, respectively). ~~A reduced number of days of POLDER-3
248 aerosol retrievals is observed in the NW-MED sub-region in November and December 2012 (respectively 11 and
249 4 days, Figure S2b), likely due to an unfavorable combination of cloudiness and spatial coverage in the
250 northernmost part of our study region during these two months. Beyond this particular case, this analysis generally~~
251 **These statistics** suggests that the cloudiness significantly reduces the number of POLDER-3 pixels available over
252 each sub-region from October to March (Figure S2a,c,e), **with more limited impact on number of available days**
253 **of POLDER-3 observations** ~~even though the number of available days of POLDER-3 observations remains~~
254 **reasonable** (Figure S2b,d,f).

255 Figure 3 illustrates the 8- or 9-year climatological mean over March 2005 – October 2013 of monthly POLDER-
256 3 derived aerosol parameters at 865 nm over the three sub-regions defined in Figure 2. The averaged seasonal
257 cycle of AOD is relatively similar over the north and central parts of the basin, whereas the southern part shows
258 generally higher total aerosol loads, and a more pronounced seasonal variability, with two maxima in April-May
259 and July (mean $AOD_{865\text{ nm}} > 0.15$). **This evolution is consistent with a dominant influence of African dust transport,**
260 **which is known to begin over the eastern basin in spring and spread over the western basin in summer (Moulin et**
261 **al., 1998; Floutsi et al, 2016).** The mean monthly variations of the POLDER-3 AOD_F integrated over the three
262 sub-regions are remarkably similar, in agreement with previous analysis based on ground-based AERONET
263 observations suggesting that the aerosol fine mode is, to some extent, relatively homogeneously distributed over
264 the western Mediterranean region (Lyamani et al., 2015; Sicard et al., 2016). Conversely, the north-south gradient
265 clearly appears for AOD_C (right column middle panel of Figure 3), especially for the SW MED area, consistently
266 with what is observed for total AOD. The seasonal variations of the monthly-averaged AE (left column middle
267 panel) reflect the north-south gradient of aerosol sizes, with an increased influence of smaller particles toward the
268 north, a pattern confirmed by the monthly evolution of FMF (left column, bottom panel). The monthly-averaged
269 AOD_{CS} (right column, bottom panel) shows very low seasonal and spatial variability, as previously observed in
270 Figure 1, whereas the POLDER-3 mean AOD_{CNS} seasonal cycle illustrates much more pronounced monthly and
271 north-south evolution, in coherence with those of AOD_C and total AOD. Figure S3 in the supplementary material
272 illustrates the climatological mean of monthly POLDER-3 AOD, AOD_F , AOD_C , and FMF extrapolated at 550 nm,
273 confirming the patterns displayed Figure 1, especially the marked increase of AOD_F values, and FMF at this
274 wavelength. **Thus, POLDER-3 FMF (550 nm) are consistent with previous averaged estimates from MODIS over**
275 **Western Mediterranean, ranging from 55 to nearly 70% (Floutsi et al., 2016).**

276 The POLDER-3 mean seasonal aerosol retrievals displayed in Figure 1 and 3 at 865 nm are summarized in Table
277 1a, those extrapolated at 550 nm (Figures S1 and S3) in Table 1b. The multi-annual averages of AOD, AOD_C and
278 AOD_{CNS} at 865 nm in Table 1a confirm the north-south gradient with minimum values in the north part (0.090,
279 0.055, and 0.043 respectively for AOD, AOD_C , and AOD_{CNS}) compared to the south part of the western
280 Mediterranean basin (0.124, 0.091, 0.073 respectively). POLDER-3 AE and FMF mean multi-annual values
281 consistently highlight an increase in the coarse component of AOD toward the south. In terms of multi-annual
282 averages, the AOD_F remains relatively uniform, with some minor variations indicating minimum fine mode
283 aerosol loads in the central area (0.032 in CW MED), maximum in the north (0.035 in NW MED) and intermediate
284 values in the south part (0.033 in SW MED), these variations being more pronounced at 550 nm (Table 1b).
285 Seasonal multi-annual averages of AOD_F highlight differences in the order of a factor 2 between minimum values

286 in the south in winter (around 0.02 at 865 nm, 0.06 at 550 nm) and maxima in spring (around 0.04 at 865 nm, and
287 0.12 at 550 nm), especially in the northern part of the region. The POLDER-3 derived mean multi-annual AOD_{CS}
288 at 865 nm (Table 1a) reveal some seasonal variability, with maximum values in summer in the south part (0.031)
289 and minimum in winter in the northern part (0.013). Although reasons for such an evolution are not fully
290 understood, considering the similarity with that of AOD_{CNS}, this variability could be partly related to the influence
291 of North African dust transport rather than fully representative of a background coarse sea-salt fraction (Claeys et
292 al., 2017). Indeed, Saharan dust might include a spherical coarse aerosol fraction following mixing with soluble
293 secondary components such as sulfate and nitrate (Drugé et al., 2019).

294 3.3 Temporal evolution at selected sites

295 The previous regional analysis is complemented by the investigation of the POLDER-3 aerosol properties around
296 three contrasted AERONET sites of the western basin: Ersa (43.00367°N, 9.35929°E, altitude 80 m), the
297 northernmost site located on northern coast of Corsica Island, France; Lampedusa (35.51667°N, 12.63167°E, alt.
298 45 m) the southernmost site located on the northwestern coast of Lampedusa Island, Italy; Barcelona (41.38925°N,
299 2.11206°E, alt. 125 m) the westernmost site located in a urban/coastal environment on the shore of northeastern
300 Spain (Figure 2). Ersa and Barcelona are sites under the influence of long-range Saharan dust transport, whereas
301 Lampedusa is subject to short to medium-range dust transport. Ersa and Lampedusa are marine background sites
302 with some anthropogenic influence, Barcelona is located in a heavily polluted environment. Ersa and Lampedusa
303 were the two super-sites of the ChArMEx (The Chemistry-Aerosol Mediterranean Experiment) collaborative
304 research program, and Barcelona, which is also part of EARLINET/ACTRIS network, one of the secondary sites
305 of this program (Mallet et al., 2016). In this context, ~~many experimental set-up of in situ aerosol measurements~~
306 ~~provided detailed aerosol characterization. Additionally,~~ the long-term AERONET routine aerosol measurements
307 at these sites have been used for the comprehensive regional validation of POLDER-3 retrievals presented in
308 Formenti et al. (2018). Here we considered the same POLDER-3 dataset, by selecting superpixels within $\pm 0.5^\circ$
309 around the AERONET sites, corresponding to a maximum number of 17 at Ersa, 28 at Lampedusa, and 13 at
310 Barcelona.

311 3.3.1 Monthly time series

312 Figure 4, 5 and 6 illustrates the month-to-month evolution from March 2005 to October 2013 of POLDER-3
313 retrievals at 865 nm, extracted at Ersa, Barcelona and Lampedusa respectively, including (a) AOD, (b) AOD_F and
314 AOD_C, (c) AOD_{CNS} and AOD_{CS}, (d) AE₈₆₅₋₆₇₀ and FMF. At these three sites, AE and FMF (Figure 4d, 5d, 6d) show
315 remarkably similar variability (correlation coefficients > 0.9), indicating that the AE is a good proxy of the
316 proportion of fine particles component relative to total AOD.

317 The average monthly FMF of the AOD at 865 nm at Ersa is estimated at 37% by POLDER-3 in all clear-sky
318 conditions, with a range of monthly mean values between 18% and 65%. Consistently, considering only the
319 POLDER-3 retrievals available in Best Viewing Conditions, the averaged repartition in terms of aerosol size mode
320 and shape contributions to the total AOD at 865 nm at Ersa are 36% for the fine AOD, 44% for the non-spherical
321 coarse mode and 20% for the spherical coarse mode.

322 As a consequence of the influence of short to medium range Saharan dust transport in Lampedusa, POLDER-3
323 AOD show their highest monthly mean values at this site (up to 0.44 in May 2011, Figure 6a), compared to both

327 Ersá (max of 0.21 in June 2007, Figure 4a) and Barcelona (max of 0.24 in June 2006, Figure 5a). These maximum
328 AOD values are clearly associated to coincident maximum values of monthly mean AOD_c, with 0.39 in May 2011
329 in Lampedusa (Figure 6b), 0.18 in June 2006 in Barcelona (Figure 5b), and 0.16 in June 2007 in Ersá (Figure 4b).
330 Figures 4-6 clearly highlight that POLDER-3 monthly mean AOD values above 0.10 are much more frequent in
331 Lampedusa (66% of frequency over the 104 months of POLDER-3 observations) than in Barcelona (43% of
332 frequency) and Ersá (30%). The contrast between the three sites is even more pronounced considering the AOD_c
333 retrievals, as the with frequencies of monthly values above 0.10 of reaching 44%, 22%, and 5% for Lampedusa,
334 Barcelona, and Ersá, respectively clearly highlights the more frequent impact of coarse particles, especially non-
335 spherical desert dust, in Lampedusa. Conversely, the monthly evolution of AOD_f reported in Figure 4b, 5b, and
336 6b does not show such a marked contrast, nor with respect to the maximum values, rather comparable at the three
337 sites (0.072, 0.074, and 0.076 in Ersá, Barcelona, and Lampedusa, respectively), or the frequency of monthly mean
338 values above 0.04 (27%, 31% and 34% respectively).

339 The months with POLDER-3 mean derived FMF greater than 50% represent a frequency of 10% over the whole
340 monthly data set in Barcelona (Figure 5d), and 0% in Lampedusa (Figure 6d). Compared to their frequency in Ersá
341 (17%, Figure 4d), POLDER-3 retrievals of fine and coarse components of AOD suggest that the influence of fine
342 particles is more frequent in Ersá, possibly due to the transport of polluted air masses from highly industrialized
343 regions (Po Valley, Marseille-Fos-Berre for example) in the north part of the basin (Mallet et al., 2016). These
344 features may could also simply reflect the more frequent high influence of desert dust at Lampedusa and in a less
345 extent at Barcelona, which may partly hide the possible influence of fine aerosols of anthropogenic origin at these
346 two sites.

347 Over the whole POLDER-3 observing period, maximum monthly mean values of AOD_{cs} range from 0.058 in Ersá
348 (March 2008, Figure 4c) to 0.075 in Lampedusa (April 2008, Figure 6c) and 0.090 in Barcelona (November 2009,
349 Figure 5c). Frequencies of monthly mean POLDER-3 AOD_{cs} values above 0.03 are 13%, 31%, and 38% at Ersá,
350 Barcelona, and Lampedusa respectively. Such a variability suggests some impact of desert dust on AOD_{cs},
351 although the contribution of sea-salt particles or a combination of both aerosol types cannot be excluded without
352 further investigations. Maximum monthly AOD_{cns} values range from 0.109 at Ersá (Sept. 2008 and May 2009,
353 Figure 4c) to 0.210 at Barcelona (Nov. 2009, Figure 5c) and 0.220 at Lampedusa (March 2005, Figure 6bc).
354 Frequencies of monthly mean POLDER-3 AOD_{cns} values above 0.03 reach 91% in Lampedusa, 70% in
355 Barcelona, and 67% in Ersá. Considering only the POLDER-3 retrievals available in Best Viewing Conditions,
356 the averaged contributions in terms of aerosol size and shapes at Barcelona are quite similar to those estimated at
357 Ersá, with 34% of fine AOD, 46% of coarse non-spherical AOD and 20% of coarse spherical AOD at 865 nm. At
358 Lampedusa, the averaged contribution of fine AOD is reduced to 26%, with a higher contribution of coarse non-
359 spherical AOD (55%), and a rather constant relative contribution of coarse spherical AOD (19%).

360
361 ~~The total aerosol load derived from POLDER 3 at this site show a marked variability, both at seasonal and~~
362 ~~interannual time scales, with a maximum recorded value of monthly averaged AOD of 0.21 (June 2007), and~~
363 ~~winter minimum values of AOD around 0.05. Monthly averaged AOD values above 0.10 occur mostly during~~
364 ~~spring (April-May) and summer (June-July) seasons. Interestingly, Figure 4a highlights some additional peak of~~
365 ~~AOD occurring in autumn for specific years, as for example in September-October 2008. Month-to-month~~
366 ~~evolution of AE and FMF reported on Figure 4d show remarkably similar variability, which confirms that the AE~~

367 is a good proxy of the proportion of fine particles component relative to total AOD. The average monthly FMF of
368 the AOD at 865 nm at Ersa is estimated at 37% by POLDER 3 in all clear sky conditions, with a range of monthly
369 mean values between 18% and 65%, and only 17 months over 103 (i.e. 17%) with FMF greater or equal to 50%
370 (considering 865 nm wavelength). These occurrences are mostly recorded in late winter (February-March) and
371 autumn (September-October-November) and are generally characterized by moderate monthly mean AOD values
372 (between 0.06 and 0.13). Figure 4b illustrates the month-to-month evolution of AOD_F and AOD_C , confirming that
373 at this wavelength (865 nm), the AOD is mostly dominated by the coarse mode fraction (63% on average). For
374 some specific months of the time series, as for example September 2005, July 2006, September 2009,
375 February/March 2010, the POLDER 3 derived AOD_F is higher than AOD_C , but these cases are rather rarely
376 observed in comparison to those corresponding to the dominance of the AOD coarse mode component. The
377 monthly evolution of POLDER 3 AOD_{CS} and AOD_{CNS} at Ersa, reported in Figure 4c also suggests a strong
378 domination of non-spherical particles in the coarse mode AOD over most of the 8.5 year time series. A few cases
379 with AOD_{CS} greater or equal to AOD_{CNS} did occur over the period, as for example in August 2010, June 2011, or
380 July 2012. They need to be explored, although they clearly do not reflect the most frequent aerosol conditions in
381 Ersa. Considering only the POLDER 3 retrievals available in Best Viewing Conditions, the averaged repartition
382 in terms of aerosol size mode and shape contributions to the total AOD at 865 nm at Ersa are 36% for the fine
383 AOD, 44% for the non-spherical coarse mode and 20% for the spherical coarse mode. These estimates are
384 consistent with the POLDER 3 data set available in all clear sky conditions, which estimate 63% of coarse mode
385 AOD versus 37% of fine mode AOD at 865 nm.

386
387 Similarly to Figure 4, Figure 5 and 6 illustrate the month-to-month evolution from March 2005 to October 2013
388 of POLDER 3 retrievals at 865 nm, extracted at Barcelona and Lampedusa respectively, including (a) AOD, (b)
389 AOD_F and AOD_C , (c) AOD_{CNS} and AOD_{CS} , (d) $AE_{865-670}$ and FMF. Consistently with the influence of short to
390 medium range Saharan dust transport expected in Lampedusa, POLDER 3 AOD show their highest monthly mean
391 values at this site (up to 0.44 in May 2011, Figure 6a), compared to both Ersa (max of 0.21 in June 2007, Figure
392 4a) and Barcelona (max of 0.24 in June 2006, Figure 5a). These maximum AOD values are clearly associated to
393 coincident maximum values of monthly mean AOD_C , with 0.39 in May 2011 in Lampedusa (Figure 6b), 0.18 in
394 June 2006 in Barcelona (Figure 5b), and 0.16 in June 2007 in Ersa (Figure 4b). Figure 4-6 clearly highlight that
395 POLDER 3 monthly mean AOD values above 0.10 are much more frequent in Lampedusa (66% of frequency
396 over the 104 months of POLDER 3 observations) than in Barcelona (43% of frequency) and Ersa (30%). The
397 contrast between the three sites is even more pronounced considering the AOD_C retrievals, as the frequency of
398 monthly values above 0.10 (44%, 22%, and 5% for Lampedusa, Barcelona, and Ersa, respectively) clearly
399 highlights the more frequent impact of coarse particles, especially non-spherical desert dust, in Lampedusa.
400 Conversely, the monthly evolution of AOD_F reported in Figure 4b, 5b, and 6b does not show such a marked
401 contrast, nor with respect to the maximum values, rather comparable at the three sites (0.072, 0.074, and 0.076 in
402 Ersa, Barcelona, and Lampedusa, respectively), or the frequency of monthly mean values above 0.04 (27%, 31%
403 and 34% respectively). At Lampedusa, monthly AOD_F are always substantially lower than monthly AOD_C (Figure
404 6b). At Barcelona monthly AOD_F are mostly below AOD_C (Figure 5b), with the noticeable exception of a few
405 months over the time period, generally in winter or late summer (Feb. 2006, Feb. 2008, Sept. 2009 for example),
406 characterized by the dominance of AOD_F . These months with POLDER 3 mean derived FMF greater than 50%
407 represent a frequency of 10% over the whole monthly data set in Barcelona (Figure 5d), and 0% in Lampedusa

408 (Figure 6d). Compared to their frequency in Ersa (17%, Figure 4d), POLDER-3 retrievals of fine and coarse
409 components of AOD suggest that the influence of fine particles is more frequent in Ersa, possibly due to the
410 transport of polluted air masses from highly industrialized regions (Po Valley, Marseille Fos Berre for example)
411 in the north part of the basin (Mallet et al., 2016). These features may also simply reflect the more frequent
412 influence of desert dust at Lampedusa and in a less extent at Barcelona, which may hide the possible influence of
413 fine aerosols of anthropogenic origin at these two sites. Over the whole POLDER-3 observing period, maximum
414 monthly mean values of AOD_{CS} range from 0.058 in Ersa (March 2008, Figure 4c) to 0.075 in Lampedusa (April
415 2008, Figure 6c) and 0.090 in Barcelona (November 2009, Figure 5c). Frequencies of monthly mean POLDER-3
416 AOD_{CS} values above 0.03 are 13%, 31%, and 38% at Ersa, Barcelona, and Lampedusa respectively. Such a
417 variability suggests some impact of desert dust on AOD_{CS}, although the contribution of sea-salt particles or a
418 combination of both aerosol types cannot be excluded without further investigations. Maximum monthly AOD_{CNS}
419 values range from 0.109 at Ersa (Sept. 2008 and May 2009, Figure 4c) to 0.210 at Barcelona (Nov. 2009, Figure
420 5b) and 0.220 at Lampedusa (March 2005, Figure 6b). Frequencies of monthly mean POLDER-3 AOD_{CNS} values
421 above 0.03 reach 91% in Lampedusa, 70% in Barcelona, and 67% in Ersa. Considering only the POLDER-3
422 retrievals available in Best Viewing Conditions, the averaged contributions in terms of aerosol size and shapes at
423 Barcelona are rather similar to those estimated at Ersa, with 34% of fine AOD, 46% of coarse non-spherical AOD
424 and 20% of coarse spherical AOD at 865 nm. At Lampedusa, the averaged contribution of fine AOD is reduced to
425 26%, with a higher contribution of coarse non-spherical AOD (55%), and a rather constant relative contribution
426 of coarse spherical AOD (19%).

427 428 3.3.2 Daily time series 429

430 Figure 7 shows the frequency distributions for daily evolution POLDER-3 AOD (a), AOD_F(b), AOD_C(c), AOD_{CNS}
431 (d), and AOD_{CS} (e) at 865 nm at Ersa, Barcelona, and Lampedusa, their daily evolutions from March 4, 2005 to
432 October 10, 2013 being reported in Figure S4 of the supplementary material of POLDER-3 AOD (a), AOD_F(b),
433 AOD_C(c), AOD_{CS}, and AOD_{CNS} (d) at 865 nm at Ersa, Barcelona, and Lampedusa. Table 2 presents a statistical
434 summary of the daily POLDER-3 aerosol retrievals for these three sites.

435 The range of AOD values varies from 0.01 to 0.68 at Ersa, 0.01 to 1.05 at Barcelona, and 0.02 to 4.72 at
436 Lampedusa, indicating the occurrence of extreme AOD events at the southernmost site of Lampedusa. Daily AOD
437 > 0.3 occur 9% of the time in Lampedusa, less than 3% of the time in Barcelona and are rare in Ersa (1.5 % of
438 frequency). At the three sites, they are characterized by the same comparable size/shape properties typical of desert
439 dust influence (mean low AE 0.31, mean and FMF, mean dominant non-spherical aerosol fraction in the coarse
440 mode of 71%). These POLDER-3 retrievals are consistent with the Gkikas et al. (2013) climatology of intense
441 desert dust events in the Mediterranean, which recorded extreme dust episodes mostly in the southern part of
442 central Mediterranean, where Lampedusa is located. ~~These authors also reported that these extreme desert dust~~
443 ~~episodes are characterized by~~ , with AOD_{550nm} values > 2.5 and up to 4.

444 The background aerosol conditions, corresponding to low POLDER-3 AOD_{865 nm} (< 0.05) show an average
445 occurrence of 22% of the time in Ersa, 20% in Barcelona and only 9.5% in Lampedusa. These features show that,
446 over the March 2005 – October 2013, POLDER-3 has recorded very low occurrence of pristine days, i.e., clean
447 conditions associated to low aerosol loads, especially at Lampedusa.

448 As reported in Table 2, the average daily AOD (865 nm) is 0.09 (standard deviation 0.07) in Ersa, 0.10 (standard
449 deviation 0.04) in Barcelona, and 0.15 (standard deviation 0.18) in Lampedusa, reflecting both higher frequency

450 and intensity of aerosol episodes in Lampedusa, as illustrated in Figure S4a 7a. This ~~main pattern~~ is also verified
451 for POLDER-3 retrievals of AOD_c and to a certain extent AOD_F, which reach their maximum values in Lampedusa
452 (4.4 and 0.35, respectively). However, POLDER-3 shows that at 865 nm, the AOD_F is always lower than 0.2
453 (Figure S4b 7b), except at Lampedusa for a reduced number of days (4). At this site, peaks of AOD_F seem to be
454 associated to peaks of AOD_C, suggesting the influence of desert dust on both aerosol size components, and/or the
455 double influence of two different aerosol types (i.e., possibly both dust and anthropogenic). POLDER-3 AOD_{CS}
456 and AOD_{CNS} time series, shown Figure S4d 7d, are more difficult to interpret, ~~first of all~~ because ~~the of~~ sampling
457 ~~is reduced~~ reduction by more than 50% compared to POLDER-3 retrievals associated to all clear sky pixels (ACSP,
458 i.e., AOD, AOD_F, AOD_C, AE), due to the necessity of best viewing conditions (BVC) for their retrieval, as reported
459 in Table 2. Despite this limitation, Figure S4d 7d and Table 2 show high variability of both spherical and non-
460 spherical aerosols in the coarse mode, with a larger range of daily values for AOD_{CNS} (up to 1.00 in Lampedusa)
461 than for AOD_{CS} (maximum 0.34 in Barcelona). ~~At the three~~ Considering the three sites considered here, POLDER-
462 3 mean retrievals of daily AOD_{CNS} (0.04 – 0.08) are on average more than two times larger than those of AOD_{CS}
463 (0.02 – 0.03).

464
465 For these days, POLDER 3 retrieves low AE (0.41 in average), low FMF (21% in average), and high contribution
466 of non-spherical aerosol fraction in the coarse mode (87% in average), consistently with the dominant influence
467 of desert dust. Such an influence is verified at Barcelona as well: although much less frequent (less than 3% of
468 occurrence), daily AOD > 0.3 are associated to average AE values of 0.44, average FMF of 21% (maximum 45%)
469 and average non-spherical aerosol fraction in the coarse mode of 85%. Finally, at Ersa POLDER 3 retrievals of
470 daily AOD > 0.3 are rare (< 2% of occurrence over the POLDER 3 observing period), and ~~characterized by the~~
471 ~~same properties typical of desert dust influence (mean AE 0.31, mean FMF 16%, mean non-spherical aerosol~~
472 ~~fraction in the coarse mode of 71%). These POLDER 3 retrievals are consistent with the Gkikas et al. (2013)~~
473 ~~climatology of intense desert dust events in the Mediterranean, which recorded extreme dust episodes mostly in~~
474 ~~the southern part of central Mediterranean, where Lampedusa is located. These authors also reported that these~~
475 ~~extreme desert dust episodes are characterized by AOD_{550nm} values > 2.5 and up to 4. At Lampedusa, Figure 7b~~
476 ~~and 7c suggest that the most intense AOD peaks are always associated to an increase in AOD_c, and in some cases~~
477 ~~in AOD_F as well. Thus, for the three main sites considered here, the aerosol retrievals recorded by POLDER 3~~
478 ~~from 2005 to 2013 highlight the high variability of both the total and the size- and shape-segregated components~~
479 ~~of the AOD.~~ The background aerosol conditions, corresponding to low POLDER-3 AOD_{865 nm} (< 0.05) show an
480 average occurrence of 22% of the time in Ersa, 20% in Barcelona and only 9.5% in Lampedusa. These features
481 show that, over the March 2005 – October 2013, POLDER-3 has recorded very low occurrence of pristine days,
482 i.e. clean conditions associated to low aerosol loads, especially at Lampedusa. ~~As reported in Table 2, the average~~
483 ~~daily AOD (865 nm) is 0.09 (standard deviation 0.07) in Ersa, 0.10 (standard deviation 0.04) in Barcelona, and~~
484 ~~0.15 (standard deviation 0.18) in Lampedusa, reflecting both higher frequency and intensity of aerosol episodes in~~
485 ~~Lampedusa, as illustrated in Figure 7a. This main pattern is also verified for POLDER-3 retrievals of AOD_c and~~
486 ~~to a certain extent AOD_F, which reach their maximum values in Lampedusa (4.4 and 0.35, respectively). However,~~
487 ~~POLDER 3 shows that at 865 nm, the AOD_F is always lower than 0.2 (Figure 7b), except at Lampedusa for a~~
488 ~~reduced number of days (4). At this site, peaks of AOD_F seem to be associated to peaks of AOD_C, suggesting the~~
489 ~~influence of desert dust on both aerosol size components, and/or the double influence of two different aerosol~~

490 types (i.e., possibly both dust and anthropogenic). POLDER-3 AOD_{CS} and AOD_{CNS} time series, shown Figure 7d,
491 are more difficult to interpret, first of all because the sampling is reduced by more than 50% compared to
492 POLDER-3 retrievals associated to all clear sky pixels (ACSP, i.e., AOD, AOD_F, AOD_C, AE), due to the necessity
493 of best viewing conditions (BVC) for their retrieval, as reported in Table 2. Despite this limitation, Figure 7d and
494 Table 2 show high variability of both spherical and non-spherical aerosols in the coarse mode, with a larger range
495 of daily values for AOD_{CNS} (up to 1.00 in Lampedusa) than for AOD_{CS} (maximum 0.34 in Barcelona). At the three
496 sites considered here, POLDER-3 mean retrievals of daily AOD_{CNS} (0.04–0.08) are on average more than two
497 times larger than those of AOD_{CS} (0.02–0.03).

498 499 **3.4 Inter-annual evolution**

500 Annual maps of POLDER-3 AOD, AOD_C, and AOD_F at 865 nm are displayed for each of the 9 available
501 observations years (2005 to 2013) in Figure 8. The annual averages are computed over the period March-October
502 only in order to consistently consider the 9 years in the whole available period. The left period November-February
503 is hopefully the period where AOD is the lowest in the region (Figure 3). Figure 8 highlights a significant
504 interannual variation in AOD (left column), characterized by elevated aerosol loads for specific years, as 2007 and
505 2008, and lower AOD ranges in 2009 and 2013. The interannual variations of POLDER-3 AOD_C (middle column)
506 tend to be relatively similar to those of AOD, especially over the south part of the basin. Figure 8 also suggests
507 that the maximum values of AOD_F (right column) were observed in the first half of the period of study, with an
508 evolution toward more moderate to low loads in fine particles apparent from 2010. Figure S4–S5 of the
509 supplementary material confirms such an evolution with annual maps of POLDER-3 AOD_F extrapolated at 550
510 nm for each of the 9 observation years. The year 2007 appears highly polluted in fine particles over the whole
511 basin. Over the most eastern part of the region, the intense plume observed by POLDER-3 can be related to the
512 occurrence of devastating fires in Greece in the summer of 2007, producing large amounts of biomass burning
513 aerosols transported downwind over the central Mediterranean (Kaskaoutis et al., 2011).

514 In order to analyze further these interannual evolutions, Figure 9 presents the time series of annual averages (~~left~~
515 ~~column~~) and monthly anomalies (~~right column~~) of POLDER-3 AOD, AOD_F, and AOD_C at 865 nm spatially
516 averaged over the north, central, and south parts of the western Mediterranean basins (~~left column~~, defined in
517 Figure 2) and extracted at Ersa, Barcelona, and Lampedusa (~~right column~~) for the period March 2005 – October
518 2013. ~~The associated~~The monthly anomalies, ~~are~~ computed by subtracting to each monthly averaged value of a
519 specific year its corresponding long-term monthly average (2005-2013) ~~are shown in Figure S6 of the~~
520 ~~supplementary material~~. Linear regressions are applied to both March-October annual averages and monthly
521 anomalies of POLDER-3 AOD, AOD_F, and AOD_C evolution as a function of time. The values of the slopes,
522 reported in Table 3 and Table 4 provide the sign and magnitude of the trends at 865 nm. Slopes derived from the
523 same analysis of POLDER-3 AOD, AOD_F, and AOD_C extrapolated at 550 nm are reported in Table S1 and Table
524 S2 of supplementary material. ~~The same approach is applied to POLDER-3 AOD, AOD_F, and AOD_C retrievals~~
525 ~~extracted at Ersa, Barcelona, and Lampedusa. Results are presented Figure 10, with trends and their statistical~~
526 ~~level of confidence reported in Table 4 at 865 nm (Table S2 of supplementary material at 550 nm).~~

527 Overall, this analysis ~~clearly~~ reveals negative values of the trends for all the sub-regions and sites considered over
528 our study region, highlighting that POLDER-3 has recorded a general decrease of aerosol loads over western
529 Mediterranean Sea over the period 2005-2013. The decreasing trends recorded for AOD interannual evolution are
530

531 found to be statistically significant, at least at the 95% confidence level, over the northern and central part of the
532 study region and, consistently, at Ersa and Barcelona (top panels of Figure 9 and 10). ~~In contrast, for the~~
533 ~~southernmost part of the region (SW MED), the 95% confidence level is not reached when considering annual~~
534 ~~means of AOD and when AOD are extracted at Lampedusa (both from annual means and monthly anomalies),~~
535 ~~suggesting more uncertainties on the robustness of the decreasing trend.~~ AOD_C interannual evolutions recorded
536 by POLDER-3 ~~show~~ suggest decreasing trends, although the confidence level of 95% is only reached when
537 considering monthly anomalies at Barcelona and for the three sub-regions (Table 3 ~~middle panels of Figure 9 and~~
538 ~~10~~). The absolute values of the POLDER-3 AOD_C decreasing trends, especially in the northern part of the basin
539 (NW MED, trend $\leq -0.0012 \text{ yr}^{-1}$) suggest a moderate-to-low decreasing tendency, around -0.01 per decade.
540 Interestingly, POLDER-3 AOD_F interannual evolutions for the three sub-regions (bottom panels of Figure 9 and
541 S6) clearly reveal robust decreasing trends, all statistically significant at 99% level (Student's test). As reported in
542 Table 3, considering the northern and central parts of the study region, AOD_F decreased by -0.0020 yr^{-1} at 865
543 nm (-0.005 yr^{-1} at 550 nm, Table S1) whereas the decrease found in the southern part is slightly lower, -0.0016
544 yr^{-1} at 865 nm ($\leq -0.004 \text{ yr}^{-1}$ at 550 nm, Table S1). ~~Analysis of~~ POLDER-3 AOD_F interannual variability at Ersa,
545 Barcelona, and Lampedusa confirm these downward evolutions, with decreasing trends statistically significant at
546 the 99% confidence level (Table 4 ~~and bottom panels of Figure 10~~). The decrease trends seem to be more
547 pronounced in Barcelona (~~\geq between -0.0026 yr^{-1} for annual means and -0.0029 yr^{-1} for monthly anomalies,~~
548 ~~respectively~~) than in Lampedusa (~~between $\geq -0.0015 \text{ yr}^{-1}$ and -0.0017 yr^{-1}~~), with intermediate magnitudes at Ersa
549 (~~between ≥ -0.0019 and -0.0024 yr^{-1}~~). Consistently, the decreasing trends derived from POLDER-3 AOD_F
550 extrapolated at 550 nm ~~very vary~~ between values around -0.007 yr^{-1} at Barcelona, $-0.005/ -0.006 \text{ yr}^{-1}$ in Ersa,
551 and -0.004 yr^{-1} in Lampedusa (Table S2). ~~The POLDER-3 AOD_F marked decreasing in Barcelona is fully~~
552 ~~consistent with surface particulate concentrations (PM) downward trend analysis in Spain provided by Querol et~~
553 ~~al. (2014) and Pandolfi et al. (2016) over comparable time periods (2001-2012 and 2004-2014 respectively).~~
554 ~~Although Querol et al. (2014) discuss effects of meteorological variability and 2008 financial crisis, their main~~
555 ~~interpretation is the effect of major policy actions on air quality.~~

556 The year-to-year variations in the North Atlantic Oscillation (NAO) have been examined in several past studies to
557 support interpretation of inter-annual changes of north African dust transport either recorded by different satellite
558 sensors, especially over the Mediterranean in the 1990s and early 2000s decades (Moulin et al., 1997; Antoine et
559 Nobileau, 2006) or simulated by regional models (Nabat et al, 2020). In the present paper, we investigate the
560 relationship between winter (December through March) NAO index defined by Hurrell (1995) and interannual
561 variations of POLDER-3 AOD, AOD_F, and AOD_C from 2005 to 2013 over the three western Mediterranean sub-
562 regions and sites considered in this work. The winter NAO indexes for the 2005–2013 period were obtained from
563 "The Climate Data Guide: Hurrell North Atlantic Oscillation (NAO) Index (station-based)"
564 (<https://climatedataguide.ucar.edu/climate-data/hurrell-north-atlantic-oscillation-nao-index-station-based>). The
565 annual means of POLDER-3 AOD and AOD_F do not show any statistically significant correlation with the winter
566 NAO Index, although the correlation coefficients for annual AOD reach 0.51 at Ersa, and 0.66 for CW MED. The
567 annual averages of AOD_C confirm a link with the NAO for the CW MED region ($r=0.70$, with 95% confidence
568 level). At Ersa, we obtain $r=0.54$ which is not significant. These correlation levels, not observed in the southern
569 areas of our study region (Lampedusa or SW MED), strongly suggest that the NAO exerts a control on north
570 African dust transport rather than on their emissions over source-regions. In order to go further, we examine the

571 relative frequency of desert dust episodes (f_D) by selecting the days associated with POLDER-3 AOD_c 865 nm \geq
572 0.10 for the three-sub regions considered in our study. Figure 14 10 reports the results for the period 2005–2013
573 (March–October) along with the time series of the winter NAO Index. A significant correlation is confirmed
574 between NAO Index and f_D for the central part of the western Mediterranean region (blue curve, $R=0.76$, with
575 95% confidence level) and to a lesser extent for the northern part of the western Mediterranean region (green
576 curve, $R=0.65$, not significant). For the southern part of the region, the correlation is much lower ($r=0.43$) although
577 some connection with NAO is apparent at the beginning of the period (2005–2009), the correlation being strongly
578 degraded by the opposition observed in 2010 between extremely low NAO index (-4.64) and a relatively high f_D
579 value (36%). It is noticeable that Salvador et al. (2014), in their analysis of interannual variations of African dust
580 outbreaks for years 2001–2011 over the western Mediterranean basin, excluded the year 2010 from their
581 correlation plots with NAO indexes considering that it was associated to an atypical low value of the NAO index,
582 most probably governed by anomalous atmospheric patterns. Interestingly, SW MED is the only of our three
583 regions where POLDER-3 has recorded a significant decreasing trend in f_D of -2% ($\pm 1\%$) per year over the period
584 2005–2013 ($R=0.68$, with 95% confident level).

585 **Conversely**, we also consider the relative frequency of occurrence of clean conditions associated to low aerosol
586 loads recorded by POLDER-3 at 865 nm for the fine fraction (daily AOD_F < 0.05, **top panels**), the coarse fraction
587 (daily AOD_C < 0.05, **middle panels**) and the total aerosol (daily AOD ≤ 0.10 , **bottom panels**), named f_{CF} (Clean
588 Fine), f_{CC} (Clean Coarse), and f_{CT} (Clean Total), respectively. Figure 12 11 reports the year-to-year evolutions of
589 f_{CF} (**top panels**), f_{CC} (**middle panels**), and f_{CT} (**bottom panels**) for the three sub-regions, NW MED, CW MED, SW
590 MED (left column) and Ersa, Barcelona, Lampedusa (right column). Clearly, POLDER-3 record an increasing
591 trend in the frequency of occurrence of clean conditions for the fine fraction of AOD, both for the three sub-regions
592 and three sites. The f_{CF} trends vary between +2% per year (SW MED and Lampedusa), +3% per year (CW MED,
593 NW MED, Ersa) and +4% per year (Barcelona), with confidence levels of 99% (except for SW MED where only
594 95% confidence level is reached). In Barcelona, the increase is spectacular with clean conditions in fine particles
595 occurring less than 60% of the time between 2005 and 2007 (minimum in 2007, with 51% of frequency) and
596 reaching values above 75% in the 2011–2013 years (maximum in 2013, with 85% of frequency). Such an evolution
597 is consistent with decreasing trends in surface PM_{2.5} at background sites in Spain and Europe reported in the
598 literature over 2002–2010 (Cusack et al., 2012). Pandolfi et al. (2016) further observed decreasing trends between
599 2004 and 2014 in northeastern Spain, both at the background site of Barcelona and at the regional background site
600 of Montseny, and mostly related them to decreases in industrial emissions and in secondary sulfate and nitrate fine
601 particle concentrations. Regarding the coarse fraction of AOD, f_{CC} records some significant year-to-year variability
602 but no tendency, except for the SW MED sub-region where a low, slightly positive trend ($< +1\%$ per year, not
603 significant) is recorded over the period 2005–2013, suggesting a possible slow evolution toward cleaner conditions
604 for the coarse aerosol fraction in the southern part of the basin. Considering the total aerosol loads (bottom panels
605 of Figure 12 11), f_{CT} evolution shows an increasing trend (between +2 and +3% per year with a 95% confidence
606 level) for the three sub-regions and three sites considered.

607 Figure 12 13 and Figure 13 14 compare the 2005–2013 (March - October) mean values of AOD_F and AOD_C
608 respectively with their anomalies for each year of the period. The year-to-year evolution of AOD_F is clearly
609 characterized by positive anomalies in the first years of the period of study (especially, 2005–2007), and negative
610 anomalies for the most recent years. The spatial **distributions** of these anomalies indicate lower than long term

611 means AOD_F over the eastern part of the region in 2012, and mostly over the northern and western part of the
612 region in 2013. Annual anomalies of AOD_C illustrated in Figure 13-14 highlight elevated loads of coarse aerosols
613 for specific years and areas of the region, as in 2008 in the southeastern part or in 2012 in the western part of the
614 basin. In contrast, 2009 (southeastern part), 2010 (western part), and 2013 (most of the basin) appear to be
615 associated with lower than long-term means values of AOD_C . These POLDER-3 interannual evolutions tend to
616 confirm the association between increased dust transport during positive NAO phases (+2.1 in 2008, +3.17 in
617 2012) and reduced dust export in negative NAO phases (-4.64 in 2010, -1.97 in 2013), ~~as previously identified in~~
618 ~~our analysis and in agreement with former studies using other satellite aerosol dataset over the region~~
619 ~~Mediterranean basin~~ (Moulin et al., 1997; Antoine and Nabileau, 2006; Papadimas et al., 2008).

620

621 4 Conclusion

622 ~~This study provides the first analysis of the spatial and temporal variability of aerosol properties obtained by the~~
623 ~~daily aerosol retrievals over the western Mediterranean Sea from the POLDER 3/PARASOL spaceborne sensor~~
624 ~~over its entire period of operation (March 2005—October 2013). With the exception of two early studies based on~~
625 ~~METEOSAT (Moulin et al., 1997; 1998) or SeaWiFS (Antoine and Nabileau, 2006), most of the previous efforts~~
626 ~~dedicated to satellite derived AOD variability analysis over the Mediterranean basin were based on MODIS data~~
627 ~~set (Papadimas et al., 2008; Floutsi et al., 2016).~~

628 On the basis of the quality and robustness of the POLDER-3 clear-sky ocean operational aerosol retrievals over
629 the western Mediterranean (Formenti et al., 2018), in this paper we investigated the spatial patterns and temporal
630 variability of the POLDER-3 AOD due in to different aerosol particle size classes (total, fine and coarse
631 components) and particle shapes (coarse spherical and non-spherical contributions) ~~in terms of spatial patterns and~~
632 ~~temporal variability over its whole observing period 2005-2013.~~

633 The POLDER-3 aerosol record confirms the high influence of north African desert dust over the region, with a
634 marked maximum in AOD, along with its coarse and coarse non-spherical component in the southernmost part of
635 the region, associated with a decrease in AE and fine mode fraction (FMF), and a seasonal maximum occurring in
636 Spring and Summer. In contrast, the coarse spherical component of AOD remains relatively homogeneously low
637 all year long over the region ($AOD_{CS} < 0.05$). The POLDER-3 retrievals of the fine component of AOD show less
638 moderate spatial variability compared to that observed for the coarse fraction, although with larger AOD_F tend to
639 be larger in the eastern part of our region of study, especially north of the Adriatic Sea.

640 ~~Seasonal averages reveal difference by a factor of 2, with minimum AOD_F of 0.02 (in winter in the south part of~~
641 ~~the region) and maximum of 0.04 (in spring in the north part of the region) at 865 nm (corresponding respectively~~
642 ~~to 0.06 and 0.12 for AOD_F at 550 nm). POLDER 3 also detects a persistent area of relatively high loads of fine~~
643 ~~particles in the northern part of the Adriatic Sea, characterized by seasonal averages of AOD_F larger than 0.12 at~~
644 ~~550 nm.~~

645 At three sites representative of different typical aerosol conditions over the western Mediterranean Sea (namely
646 Ersa, Barcelona, and Lampedusa), POLDER-3 retrievals at 865 nm indicate averages contributions to total AOD
647 at 865 nm ranging between 19 and 20% for coarse spherical particles, 26 and 36% for fine particles (maximum at
648 Ersa), and 44 and 55% for coarse non-spherical particles (maximum at Lampedusa). At Lampedusa, POLDER-3
649 daily observations record the occurrence of intense or extreme aerosol events ($AOD > 1$ up to 4.7) consistently
650 with the higher and more direct influence of severe desert dust episodes at this southernmost site. At these three

651 sites, daily POLDER-3 AOD_{865 nm} values above 0.3 are associated with low AE and FMF fraction (mean values
652 below 0.5 and 21%, respectively), as well as a dominance of the non-spherical particle fraction in the coarse mode
653 (mean values above 71%), typical of the desert dust influence. The background “clean” conditions associated to
654 very low aerosol loads (POLDER-3 daily AOD_{865 nm} values below 0.05) occur 22% of the time around Ersa, 20%
655 around Barcelona and 9.5% around Lampedusa over the POLDER-3 period (2005-2013), highlighting the scarcity
656 of pristine days in this region, especially in its southern part.

657 ~~Our analysis shows that the~~ interannual evolutions of ~~March to October POLDER-3-derived~~ AOD, AOD_F and
658 AOD_C ~~reveal have~~ negative trends over the period 2005-2013, ~~these trends being~~ more pronounced in time and
659 ~~space for AOD, and above all for~~ AOD_F, than for the AOD_C/AOD components. On average the POLDER-3 AOD
660 decreased by 0.0030 per year at 865 nm (0.0060 per year at 550 nm) over most of the region, with high
661 contributions of decreasing fine mode AOD (-0.0020 per year at 865 nm, -0.0050 per year at 550 nm). These
662 decreasing tendencies are consistent with those reported in previous studies based on MODIS AOD at 550 nm,
663 ranging from -0.0030 per year (over 2002-2014, Floutsi et al., 2016) and -0.0067 per year (over 2000-2006,
664 Papadimas et al., 2008).

665 ~~Further analysis suggests~~ We suggest a link between inter-annual evolution of winter NAO Index and frequency
666 of desert dust episodes (POLDER-3 AOD_C at 865 nm greater than 0.10, f_D), especially ~~significant in~~ over the
667 central part of the western Mediterranean Sea, along with a possible moderate diminution of frequency of dust
668 spatially limited to the south basin, as also indicated by Floutsi et al. (2016).

669 Our results strongly support the significant improvement in air quality for the fine mode aerosol component over
670 the western Mediterranean region, with much less evidence of such a large-scale evolution for the coarse fraction.
671 POLDER-3 analysis shows that aerosol year-to-year evolution over the period 2005-2013 is marked by significant
672 positive trends of occurrences of clean conditions in terms of fine particles (classified as AOD_F 865 nm below
673 0.05), between +2 and +4% per year over the whole region. In Barcelona, for instance, clean conditions recorded
674 by POLDER-3 AOD_F were as frequent as 75% in the period 2010-2013.

675
676 ~~The analysis of the evolution of clean conditions considering both coarse and fine aerosol components recorded~~
677 ~~by POLDER 3 over the period March 2005—October 2013 highlights significant positive trends for clean~~
678 ~~conditions in terms of fine particles (between +2 and +4% per year) over the region, whereas no tendency is evident~~
679 ~~for the year-to-year evolution of clean conditions for coarse particles. It is noticeable that the annual frequency of~~
680 ~~occurrence of clean conditions relative to fine particles reaches values above 75–80% in Ersa and Barcelona in the~~
681 ~~last part of the POLDER 3 operation time, i.e. over the years 2010–2013. These values are much above those~~
682 ~~retrieved in the beginning of POLDER 3 record (< 57% in Barcelona and < 67% in Ersa) over the years 2005–~~
683 ~~2007. Thus, POLDER 3 aerosol dataset analysis strongly suggests a significant improvement in air quality for the~~
684 ~~fine mode aerosol component over the western Mediterranean region, consistent with decreasing anthropogenic~~
685 ~~emissions and surface PM_{2.5} reported in Europe around the same period. The occurrence of clean conditions in~~
686 ~~terms of coarse aerosol component, with no significant detected tendency, is overall less frequent over our region~~
687 ~~of study, with annual values generally below 50–60%, highlighting the large regional influence of desert dust~~
688 ~~transported from north African sources.~~

689 ~~In conclusion, the high-resolved long-time series POLDER-3 data set of AOD of different size classes provides~~
690 ~~new and independent insights complementing previous climatology analysis and trend, which, to date, are largely~~
691 ~~based on the MODIS long-term satellite dataset (e.g. Papadimas et al., 2008; Floutsi et al., 2016).~~

692 Overall, our analysis contributes to emphasize the capacity of evolved aerosol dedicated satellite datasets in
693 distinguishing multi-influenced pluri-annual evolutions in regions undergoing complex aerosol contributions, as
694 in the Mediterranean basin. Such an approach may be investigated in other climate-sensitive regions of the world,
695 subjected to specific anthropogenic pressures and meteorological patterns. In the Mediterranean, this POLDER-3
696 data set will be part of the validation exercise of regional climate model analysis in the framework of the Flagship
697 Pilot Studies of aerosols within CORDEX (Nabat et al., 2013; 2020).

698 ~~The integration of the POLDER-3 dataset should be most useful as a complement to climate regional model aerosol~~
699 ~~analysis (Nabat et al., 2013; 2020) for better constraining the evolution and impacts of the variety of aerosols~~
700 ~~present in the Mediterranean atmosphere.~~

701 ~~In addition, based on the series of POLDER missions, the capability of multi-spectral, multi-directional and multi-~~
702 ~~polarization observations, associated with new inversion schemes, to retrieve aerosol optical and microphysical~~
703 ~~properties has been successfully proved (Dubovik et al., 2019). Growing attention to polarization observations has~~
704 ~~resulted in the 3MI instrument that enhances the POLDER concept with more spectral information and a better~~
705 ~~spatial resolution (Fougnie et al., 2018).~~

706 It is noticeable that the annual frequency of occurrence of clean conditions relative to fine particles reaches values
707 above 75–80% in Ersea and Barcelona in the last part of the POLDER-3 operation time, i.e. over the years 2010–
708 2013. These values are much above those retrieved in the beginning of POLDER-3 record (< 57% in Barcelona
709 and < 67% in Ersea) over the years 2005–2007. Thus, POLDER-3 aerosol dataset analysis strongly suggests a
710 significant improvement in air quality for the fine mode aerosol component over the western Mediterranean region,
711 consistent with decreasing anthropogenic emissions and surface PM_{2.5} reported in Europe around the same period.

712

713 **Data availability**

714 POLDER-3 data extraction was performed with the program PARASOLASCI (http://www-loa.univ-
715 lille1.fr/~ducos/public/parasolascii/). This version is made available from the AERIS Data and Service Center
716 (http://www.icare.univ-lille1.fr/parasol). Technical details are described at http://www.icare.univ-
717 lille1.fr/projects_data/parasol/docs/Parasol_Level-2_format_latest.pdf. The definition of the flag index is detailed
718 at page 18 (parameter: quality of the fit).

719 **Competing interests**

720 FD is guest editor for the ACP Special Issue of the Chemistry and Aerosols Mediterranean Experiment (ChArMEx)
721 (ACP/AMT inter-journal SI)". The remaining authors declare that they have no conflict of interest.

722 **Special issue statement**

723 This article is part of the special issue of the Chemistry and Aerosols Mediterranean Experiment (ChArMEx)
724 (ACP/AMT inter-journal SI)". It is not associated with a conference.

725 **Acknowledgements**

726 This work is part of the ChArMEx project supported by CNRS-INSU, ADEME, Météo-France and CEA in the
727 framework of the multidisciplinary program MISTRALS (Mediterranean Integrated Studies at Regional And
728 Local Scales; http://mistrals-home.org/). It has also been supported by the French National Research Agency

729 (ANR) through the ADRIMED project (contract ANR-11-BS56-0006) and by the French National Program of
730 Spatial Teledetection (PNTS, <http://www.insu.cnrs.fr/pnts>, project n°PNTS-2015-03). L. Mbemba Kabuiku was
731 granted by the French Environment and Energy Management Agency (ADEME) and National Center of Space
732 Studies (CNES). The French national center for Atmospheric data and services AERIS provided access to the
733 POLDER-3 data used.

734 LOA participates in the CaPPA (Chemical and Physical Properties of the Atmosphere) project funded by the
735 French National Research Agency (ANR) through the PIA (Programme d'Investissement d'Avenir) under contract
736 ANR-11-LABX-0005-01, the Regional Council "Hauts-de-France" and the European Regional Development
737 Fund (ERDF). We would like to thank Marc Mallet and Pierre Nabat (CNRM-Toulouse, France) for fruitful
738 discussions about the results of this paper.

739

740 **References**

741 Ancellet, G., Pelon, J., Totems, J., Chazette, P., Bazureau, A., Sicard, M., Di Iorio, T., Dulac, F., and Mallet, M.:
742 Long-range transport and mixing of aerosol sources during the 2013 North American biomass burning episode:
743 analysis of multiple lidar observations in the western Mediterranean basin, *Atmos. Chem. Phys.*, 16, 4725-4742,
744 <https://doi.org/10.5194/acp-16-4725-2016>, 2016.

745 Antoine, D., and Nobileau, D.: Recent increase of Saharan dust transport over the Mediterranean Sea, as revealed
746 from ocean color satellite (SeaWiFS) observations, *J. Geophys. Res. Atmos.*, 111, 1–19,
747 <https://doi.org/10.1029/2005JD006795>, 2006.

748 Barnaba, F., and Gobbi, G. P.: Aerosol seasonal variability over the Mediterranean region and relative impact of
749 maritime, continental and Saharan dust particles over the basin from MODIS data in the year 2001, *Atmos. Chem.*
750 *Phys.*, 4, 2367–2391, <https://doi.org/10.5194/acp-4-2367-2004>, 2004.

751 Boucher, O.: *Atmospheric Aerosols - Properties and Climate Impacts*, 311 pp., Springer,
752 <https://doi.org/10.1007/978-94-017-9649-1>, 2015.

753 Bréon, F. M., Vermeulen, A., and Descloitres, J.: An evaluation of satellite aerosol products against sunphotometer
754 measurements, *Remote Sens. Environ.*, 115, 3102–3111, <https://doi.org/10.1016/j.rse.2011.06.017>, 2011.

755 Chazette, P., Totems, J., Ancellet, G., Pelon, J., and Sicard, M.: Temporal consistency of lidar observables during
756 aerosol transport events in the framework of the ChArMEx/ADRI-MED campaign at Menorca Island in June 2013,
757 *Atmos. Chem. Phys.*, 16, 2863–2875, <https://doi.org/10.5194/acp-16-2863-2016>, 2016.

758 Chazette, P., Totems, J., and Shang, X.: Transport of aerosols over the French Riviera - link between ground-based
759 lidar and spaceborne observations, *Atmos. Chem. Phys.*, 19, 3885-3904, [https://doi.org/10.5194/acp-19-3885-](https://doi.org/10.5194/acp-19-3885-2019)
760 [2019](https://doi.org/10.5194/acp-19-3885-2019), 2019.

761 Chrit, M., Sartelet, K., Sciare, J., Pey, J., Nicolas, J. B., Marchand, N., Freney, E., Sellegri, K., Beckmann, M.,
762 and Dulac, F.: Aerosol sources in the western Mediterranean during summertime: A model-based approach, *Atmos.*
763 *Chem. Phys.*, 18, 9631-9659, <https://doi.org/10.5194/acp-18-9631-2018>, 2018.

764 Claeys, M., Roberts, G., Mallet, M., Arndt, J., Sellegri, K., Sciare, J., Wenger, J., and Sauvage, B.: Optical,
765 physical and chemical properties of aerosols transported to a coastal site in the western Mediterranean: a focus on
766 primary marine aerosols, *Atmos. Chem. Phys.*, 17, 7891–7915, <https://doi.org/10.5194/acp-17-7891-2017>, 2017.

767 Cusack, M., Alastuey, A., Pérez, N., Pey, J., and Querol, X.: Trends of particulate matter (PM_{2.5}) and chemical
768 composition at a regional background site in the Western Mediterranean over the last nine years (2002–2010),
769 *Atmos. Chem. Phys.*, 12, 8341–8357, <https://doi.org/10.5194/acp-12-8341-2012>, 2012.

770 Denjean, C., Cassola, F., Mazzino, A., Triquet, S., Chevaillier, S., Grand, N., Bourriane, T., Momboisse, G.,
771 Sellegri, K., Schwarzenbock, A., Freney, E., Mallet, M., and Formenti, P.: Size distribution and optical properties
772 of mineral dust aerosols transported in the western Mediterranean. *Atmos. Chem. Phys.*, 16, 1081–1104,
773 <https://doi.org/10.5194/acp-16-1081-2016>, 2016.

774 Di Biagio, C., Doppler, L., Gaimoz, C., Grand, N., Ancellet, G., Raut, J.-C., Beekmann, M., Borbon, A., Sartelet,
775 K., Attié, J.-L., Ravetta, F., and Formenti, P.: Continental pollution in the western Mediterranean basin: vertical
776 profiles of aerosol and trace gases measured over the sea during TRAQA 2012 and SAFMED 2013, *Atmos. Chem.*
777 *Phys.*, 15, 9611–9630, <https://doi.org/10.5194/acp-15-9611-2015>, 2015.

778 Di Biagio, C., Formenti, P., Doppler, L., Gaimoz, C., Grand, N., Ancellet, G., Attié, J.-L., Bucci, S., Dubuisson,
779 P., Fierli, F., Mallet, M., and Ravetta, F.: Continental pollution in the Western Mediterranean basin: large
780 variability of the aerosol single scattering albedo and influence on the direct shortwave radiative effect, *Atmos.*
781 *Chem. Phys.*, 16, 10591–10607, <https://doi.org/10.5194/acp-16-10591-2016>, 2016.

782 Drugé, T., Nabat, P., Mallet, M., and Somot, S.: Model simulation of ammonium and nitrate aerosols distribution
783 in the Euro-Mediterranean region and their radiative and climatic effects over 1979–2016, *Atmos. Chem. Phys.*,
784 19, 3707–3731, <https://doi.org/10.5194/acp-19-3707-2019>, 2019.

785 [Dubovik, O., Li, Z., Mishchenko, M. I., Tanré, D., Karol, Y., Bojkov, B., Cairns, B., Diner, D. J., Espinosa, W.](#)
786 [R., Goloub, P., Gu, X., Hasekamp, O., Hong, J., Hou, W., Knobelspiesse, K. D., Landgraf, J., Li, L., Litvinov, P.,](#)
787 [Liu, Y., Lopatin, A., Marbach, T., Maring, H., Martins, V., Meijer, Y., Milinevsky, G., Mukai, S., Parol, F., Qiao,](#)
788 [Y., Remer, L., Rietjens, J., Sano, I., Stammes, P., Stammes, S., Sun, X., Tabary, P., Travis, L. D., Waquet, F., Xu,](#)
789 [F., Yan, C. and Yin, D.: Polarimetric remote sensing of atmospheric aerosols: Instruments, methodologies, results,](#)
790 [and perspectives, *J. Quant. Spectrosc. Radiat. Transf.*, 224, 474–511, doi:10.1016/j.jqsrt.2018.11.024, 2019.](#)

791 Dubovik, O., Sinyuk, A., Lapyonok, T., Holben, B. N., Mishchenko, M., Yang, P., Eck, T. F., Volten, H., Muñoz,
792 O., Veihelmann, B., van der Zande, W. J., Leon, J.-F., Sorokin, M., and Slutsker, I.: Application of spheroid
793 models to account for aerosol particle nonsphericity in remote sensing of desert dust, *J. Geophys. Res.*, 111,
794 D11208, <https://doi.org/10.1029/2005JD006619>, 2006.

795 Dulac, F., Tanré, D., Bergametti, G., Buat-Ménard, P., Desbois, M., and Sutton, D.: Assessment of the African
796 airborne dust mass over the western Mediterranean Sea using Meteosat data, *J. Geophys. Res.*, 97, 2489–2506,
797 <https://doi.org/10.1029/91JD02427>, 1992.

798 Floutsi, A.A., M.B. Korras-Carraca, C. Matsoukas, N. Hatzianastassiou, and G. Biskos, Climatology and trends
799 of aerosol optical depth over the Mediterranean basin during the last 12 years (2002–2014) based on Collection
800 006 MODIS-Aqua data, *Sci. Total Environ.*, 551–552, 292–293, <https://doi.org/10.1016/j.scitotenv.2016.01.192>,
801 2016.

802 Formenti, P. (Coord.), Mediterranean aerosol properties, Part VII in: Mediterranean Atmospheric Chemistry in the
803 Mediterranean – Vol. 2, From Pollutant Sources to Impacts, Dulac, F., Sauvage, S., and Eric Hamonou (Eds.),
804 Springer, in prep., 2020.

805 Formenti, P., Mbemba Kabuiku, L., Chiapello, I., Ducos, F., Dulac, F., and Tanré, D.: Aerosol optical properties
806 derived from POLDER-3/PARASOL (2005–2013) over the western Mediterranean Sea – Part 1: Quality

807 assessment with AERONET and in situ airborne observations, *Atmos. Meas. Tech.*, 11, 6761–6784,
808 <https://doi.org/10.5194/amt-11-6761-2018>, 2018.

809 Fougnie, B., Improvement of the PARASOL Radiometric In-Flight Calibration Based on Synergy Between
810 Various Methods Using Natural Targets, in *IEEE Transactions on Geoscience and Remote Sensing*, vol. 54, no.
811 4, pp. 2140-2152, April 2016, doi: 10.1109/TGRS.2015.2496322, 2016.

812 ~~Fougnie, B., Marbach, T., Lacan, A., Lang, R., Schlüssel, P., Poli, G., Munro, R. and Couto, A. B.: The multi-~~
813 ~~viewing multi-channel multi-polarisation imager—Overview of the 3MI polarimetric mission for aerosol and cloud~~
814 ~~characterization, *J. Quant. Spectrosc. Radiat. Transf.*, 219, 23–32, doi:10.1016/j.jqsrt.2018.07.008, 2018.~~

815 Georgoulas, A. K., Alexandri, G., Kourtidis, K. A., Lelieveld, J., Zanis, P., Pöschl, U., Levy, R., Amiridis, V.,
816 Marinou, E., and Tsikerdekis, A.: Spatiotemporal variability and contribution of different aerosol types to the
817 aerosol optical depth over the Eastern Mediterranean, *Atmos. Chem. Phys.*, 16, 13853–13884,
818 <https://doi.org/10.5194/acp-16-13853-2016>, 2016.

819 Gkikas, A., Basart, S., Hatzianastassiou, N., Marinou, E., Amiridis, V., Kazadzis, S., Pey, J., Querol, X., Jorba,
820 O., Gassó, S., and Baldasano, J. M.: Mediterranean intense desert dust outbreaks and their vertical structure based
821 on remote sensing data, *Atmos. Chem. Phys.*, 16, 8609–8642, <https://doi.org/10.5194/acp-16-8609-2016>, 2016.

822 Gkikas, A., Hatzianastassiou, N., Mihalopoulos, N., Katsoulis, V., Kazadzis, S., Pey, J., Querol, X., and Torres,
823 O.: The regime of intense desert dust episodes in the Mediterranean based on contemporary satellite observations
824 and ground measurements, *Atmos. Chem. Phys.*, 13, 12135–12154, <https://doi.org/10.5194/acp-13-12135-2013>,
825 2013.

826 **Hansson, H.-C.; Tunved, P.; Krejci, R.; Freud, E.; Kalivitis, N.; Hennig, T.; Maneas, G.; Gerasopoulos, E. The**
827 **Atmospheric Aerosol over Western Greece-Six Years of Aerosol Observations at the Navarino Environmental**
828 **Observatory. *Atmosphere*, 12, 445. <https://doi.org/10.3390/atmos12040445>, 2021.**

829 Hatzianastassiou, N., A. Gkikas, N. Mihalopoulos, O. Torres, and B. D. Katsoulis (2009), Natural versus
830 anthropogenic aerosols in the eastern Mediterranean basin derived from multiyear TOMS and MODIS satellite
831 data, *J. Geophys. Res.*, 114, D24202, <https://doi.org/10.1029/2009JD011982>.

832 Herman, M., Deuzé, J. L., Marchand, A., Roger, B., and Lallart, P.: Aerosol remote sensing from
833 POLDER/ADEOS over the ocean: Improved retrieval using a nonspherical particle model, *J. Geophys. Res.*, 110,
834 D10S02, <https://doi.org/10.1029/2004JD004798>, 2005.

835 Holben, B. N., Tanré, D., Smirnov, A., Eck, T. F., Slutsker, I., Abuhassan, N., Newcomb, W. W., Schafer, J. S.,
836 Chatenet, B., Lavenue, F., Kaufman, Y. J., Castle, J. Vande, Setzer, A., Markham, B., Clark, D., Frouin, R.,
837 Halthore, R., Karneli, A., O'Neill, N. T., Pietras, C., Pinker, R. T., Voss, K., and Zibordi, G.: An emerging ground-
838 based aerosol climatology: Aerosol optical depth from AERONET, *J. Geophys. Res. Atmos.*, 106, 12067–12097,
839 <https://doi.org/10.1029/2001JD900014>, 2001.

840 Hurrell, J. W., Decadal trend in the North Atlantic Oscillation: Regional temperatures and precipitations, *Science*,
841 269, 676–679, <https://doi.org/10.1126/science.269.5224.676>, 1995.

842 Kaskaoutis D. G., Shailesh Kumar Kharol, N. Sifakis, P.T. Nastos, Anu Rani Sharma, K.V.S. Badarinath, H.D.
843 Kambezidis, Satellite monitoring of the biomass-burning aerosols during the wildfires of August 2007 in Greece:
844 Climate implications, *Atmospheric Environment*, Volume 45, Issue 3, Pages 716-726,
845 <https://doi.org/10.1016/j.atmosenv.2010.09.043>, 2011.

846 Laj, P., Klausen, J., Bilde, M., Plass-Duelmer, C., Pappalardo, G., Clerbaux, C., Baltensperger, U., Hjorth, J.,
847 Simpson, D., Reimann, S. and Coheur, P. F.: Measuring atmospheric composition change, *Atmos. Environ.*, 43,
848 5351–5414, <https://doi.org/10.1016/j.atmosenv.2009.08.020>, 2009.

849 Laj, P., Bigi, A., Rose, C., Andrews, E., Lund Myhre, C., Collaud Coen, M., Lin, Y., Wiedensohler, A., Schulz,
850 M., Ogren, J. A., Fiebig, M., Glib, J., Mortier, A., Pandolfi, M., Petäjä, T., Kim, S.-W., Aas, W., Putaud, J.-P.,
851 Mayol-Bracero, O., Keywood, M., Labrador, L., Aalto, P., Ahlberg, E., Alados Arboledas, L., Alastuey, A.,
852 Andrade, M., Artíñano, B., Ausmeel, S., Arsov, T., Asmi, E., Backman, J., Baltensperger, U., Bastian, S., Bath,
853 O., Beukes, J. P., Brem, B. T., Bukowiecki, N., Conil, S., Couret, C., Day, D., Dayantolis, W., Degorska, A.,
854 Eleftheriadis, K., Fetfatzis, P., Favez, O., Flentje, H., Gini, M. I., Gregorič, A., Gysel-Beer, M., Hallar, A. G.,
855 Hand, J., Hoffer, A., Hueglin, C., Hooda, R. K., Hyvärinen, A., Kalapov, I., Kalivitis, N., Kasper-Giebl, A., Kim,
856 J. E., Kouvarakis, G., Kranjc, I., Krejci, R., Kulmala, M., Labuschagne, C., Lee, H.-J., Lihavainen, H., Lin, N.-H.,
857 Löschau, G., Luoma, K., Marinoni, A., Martins Dos Santos, S., Meinhardt, F., Merkel, M., Metzger, J.-M.,
858 Mihalopoulos, N., Nguyen, N. A., Ondracek, J., Pérez, N., Perrone, M. R., Petit, J.-E., Picard, D., Pichon, J.-M.,
859 Pont, V., Prats, N., Prenni, A., Reisen, F., Romano, S., Sellegri, K., Sharma, S., Schauer, G., Sheridan, P., Sherman,
860 J. P., Schütze, M., Schwerin, A., Sohmer, R., Sorribas, M., Steinbacher, M., Sun, J., Titos, G., Toczko, B., Tuch,
861 T., Tulet, P., Tunved, P., Vakkari, V., Velarde, F., Velasquez, P., Villani, P., Vratolis, S., Wang, S.-H., Weinhold,
862 K., Weller, R., Yela, M., Yus-Diez, J., Zdimal, V., Zieger, P., and Zikova, N.: A global analysis of climate-relevant
863 aerosol properties retrieved from the network of Global Atmosphere Watch (GAW) near-surface observatories,
864 *Atmos. Meas. Tech.*, 13, 4353–4392, <https://doi.org/10.5194/amt-13-4353-2020>, 2020.

865 Lelieveld, J., Berresheim, H., Borrmann, S., Crutzen, P. J., Dentener, F. J., Fischer, H., Feichter, J., Flatau, P. J.,
866 Heland, J., Holzinger, R., Kormann, R., Lawrence, M. G., Levin, Z., Markowicz, K. M., Mihalopoulos, N.,
867 Minikin, a, Ramanathan, V., De Reus, M., Roelofs, G. J., Scheeren, H. a, Sciare, J., Schlager, H., Schultz, M.,
868 Siegmund, P., Steil, B., Stephanou, E. G., Stier, P., Traub, M., Warneke, C., Williams, J., and Ziereis, H.: Global
869 air pollution crossroads over the Mediterranean, *Science*, 298, 794–9, <https://doi.org/10.1126/science.1075457>,
870 2002.

871 Lyamani, H., Valenzuela, A., Perez-Ramirez, D., Toledano, C., Granados-Muñoz, M. J., Olmo, F. J., and Alados-
872 Arboledas, L.: Aerosol properties over the western Mediterranean basin: temporal and spatial variability, *Atmos.*
873 *Chem. Phys.*, 15, 2473–2486, <https://doi.org/10.5194/acp-15-2473-2015>, 2015.

874 Mallet, M., Dulac, F., Formenti, P., Nabat, P., Sciare, J., Roberts, G., Pelon, J., Ancellet, G., Tanré, D., Parol, F.,
875 Denjean, C., Brogniez, G., di Sarra, A., Alados-Arboledas, L., Arndt, J., Auriol, F., Blarel, L., Bourrienne, T.,
876 Chazette, P., Chevaillier, S., Claeys, M., D'Anna, B., Derimian, Y., Desboeufs, K., Di Iorio, T., Doussin, J.-F.,
877 Durand, P., Féron, A., Freney, E., Gaimoz, C., Goloub, P., Gómez-Amo, J. L., Granados-Muñoz, M. J., Grand,
878 N., Hamonou, E., Jankowiak, I., Jeannot, M., Léon, J.-F., Maillé, M., Mailler, S., Meloni, D., Menut, L.,
879 Momboisse, G., Nicolas, J., Podvin, T., Pont, V., Rea, G., Renard, J.-B., Roblou, L., Schepanski, K.,
880 Schwarzenboeck, A., Sellegri, K., Sicard, M., Solmon, F., Somot, S., Torres, B., Totems, J., Triquet, S., Verdier,
881 N., Verwaerde, C., Waquet, F., Wenger, J., and Zapf, P.: Overview of the Chemistry-Aerosol Mediterranean
882 Experiment/Aerosol Direct Radiative Forcing on the Mediterranean Climate (ChArMEx/ADRMED) summer
883 2013 campaign, *Atmos. Chem. Phys.*, 16, 455-504, <https://doi.org/10.5194/acp-16-455-2016>, 2016.

884 Menut, L., Siour, G., Mailler, S., Couvidat, F., and Bessagnet, B.: Observations and regional modeling of aerosol
885 optical properties, speciation and size distribution over northern Africa and western Europe, *Atmos. Chem. Phys.*,
886 16, 12961–12982, <https://doi.org/10.5194/acp-16-12961-2016>, 2016.

887 Michoud, V., Sciare, J., Sauvage, S., Dusanter, S., Léonardis, T., Gros, V., Kalogridis, C., Zannoni, N., Féron, A.,
888 Petit, J.-E., Crenn, V., Baisnée, D., Sarda-Estève, R., Bonnaire, N., Marchand, N., DeWitt, H. L., Pey, J., Colomb,
889 A., Gheusi, F., Szidat, S., Stavroulas, I., Borbon, A., and Locoge, N.: Organic carbon at a remote site of the western
890 Mediterranean Basin: composition, sources and chemistry during the ChArMEx SOP2 field experiment, *Atmos.*
891 *Chem. Phys.*, 17, 8837–8865, <https://doi.org/10.5194/acp-17-8837-2017>, 2017.

892 Moulin, C., Lambert, C. E., Dayan, U., Masson, V., Ramonet, M., Bousquet, P., Legrand, M., Balkanski, Y. J.,
893 Guelle, W., Marticorena, B., Bergametti, G., and Dulac, F.: Satellite climatology of African dust transport in the
894 Mediterranean atmosphere, *J. Geophys. Res.*, 103, 13137, doi:10.1029/98JD00171, 1998.

895 Moulin, C., Lambert, C. E., Dulac, F., and Dayan, U.: Control of atmospheric export of dust from North Africa by
896 the North Atlantic Oscillation, *Nature*, 387, 691–694, <https://doi.org/10.1038/42679>, 1997.

897 Nabat, P., Somot, S., Cassou, C., Mallet, M., Michou, M., Bouniol, D., Decharme, B., Drugé, T., Roehrig, R., and
898 Saint-Martin, D.: Modulation of radiative aerosols effects by atmospheric circulation over the Euro-Mediterranean
899 region, *Atmos. Chem. Phys.*, 20, 8315–8349, <https://doi.org/10.5194/acp-20-8315-2020>, 2020.

900 Nabat, P., Somot, S., Mallet, M., Chiapello, I., Morcrette, J. J., Solmon, F., Szopa, S., Dulac, F., Collins, W., Ghan,
901 S., Horowitz, L. W., Lamarque, J. F., Lee, Y. H., Naik, V., Nagashima, T., Shindell, D., and Skeie, R.: A 4-D
902 climatology (1979-2009) of the monthly tropospheric aerosol optical depth distribution over the Mediterranean
903 region from a comparative evaluation and blending of remote sensing and model products, *Atmos. Meas. Tech.*,
904 6, 1287–1314, doi:10.5194/amt-6-1287-2013, 2013.

905 Pandolfi, M., Alastuey, A., Pérez, N., Reche, C., Castro, I., Shatalov, V., and Querol, X.: Trends analysis of PM
906 source contributions and chemical tracers in NE Spain during 2004–2014: a multi-exponential approach, *Atmos.*
907 *Chem. Phys.*, 16, 11787–11805, <https://doi.org/10.5194/acp-16-11787-2016>, 2016.

908 Pandolfi, M., Alados-Arboledas, L., Alastuey, A., Andrade, M., Angelov, C., Artiñano, B., Backman, J.,
909 Baltensperger, U., Bonasoni, P., Bukowiecki, N., Collaud Coen, M., Conil, S., Coz, E., Crenn, V., Dudoitis, V.,
910 Ealo, M., Eleftheriadis, K., Favez, O., Fetfatzis, P., Fiebig, M., Flentje, H., Ginot, P., Gysel, M., Henzing, B.,
911 Hoffer, A., Holubova Smejkalova, A., Kalapov, I., Kalivitis, N., Kouvarakis, G., Kristensson, A., Kulmala, M.,
912 Lihavainen, H., Lunder, C., Luoma, K., Lyamani, H., Marinoni, A., Mihalopoulos, N., Moerman, M., Nicolas, J.,
913 O'Dowd, C., Petäjä, T., Petit, J.-E., Pichon, J. M., Prokopciuk, N., Putaud, J.-P., Rodríguez, S., Sciare, J., Sellegri,
914 K., Swietlicki, E., Titos, G., Tuch, T., Tunved, P., Ulevicius, V., Vaishya, A., Vana, M., Virkkula, A., Vratolis,
915 S., Weingartner, E., Wiedensohler, A., and Laj, P.: A European aerosol phenomenology – 6: scattering properties
916 of atmospheric aerosol particles from 28 ACTRIS sites, *Atmos. Chem. Phys.*, 18, 7877–7911,
917 <https://doi.org/10.5194/acp-18-7877-2018>, 2018.

918 Papadimas, C. D., Hatzianastassiou, N., Mihalopoulos, N., Querol, X., and Vardavas, I.: Spatial and temporal
919 variability in aerosol properties over the Mediterranean basin based on 6- year (2000–2006) MODIS data: *J.*
920 *Geophys. Res.*, 113, D11205, <https://doi.org/10.1029/2007JD009189>, 2008.

921 Querol X., Alastuey A., Pandolfi M., Reche C., Pérez N., Minguillón M.C., Moreno T., Viana M., Escudero M.,
922 Orío A., Pallarés M., Reina F.: 2001-2012 trends on air quality in Spain, *Sci Total Environ.*, Aug 15;490:957-69.
923 doi: 10.1016/j.scitotenv.2014.05.074.2014.

924 Rea, G., Turquety, S., Menut, L., Briant, R., Mailler, S., and Siour, G.: Source contributions to 2012 summertime
925 aerosols in the Euro-Mediterranean region, *Atmos. Chem. Phys.*, 15, 8013–8036, doi:10.5194/acp-15-8013-2015,
926 2015.

927 Remer, L.R., R. C. Levy, S. Mattoo, D. Tanré, P. Gupta, Y. Shi, V. Sawyer, L. A. Munchak, Y. Zhou, M. Kim, C.
928 Ichoku, F. Patadia, R.-R. Li, S. Gassó, R. G. Kleidman, and B. N. Holben, The Dark Target Algorithm for
929 Observing the Global Aerosol System: Past, Present, and Future, *Remote Sens.* 2020, 12, 2900 ;
930 doi :10.3390/rs12182900,2020.

931 Ricaud, P., Zbinden, R., Catoire, V., Brocchi, V., Dulac, F., Hamonou, E., Canonici, J.-C., El Amraoui, L.,
932 Massart, S., Pignatelli, B., Dayan, U., Nabat, P., Sciare, J., Ramonet, M., Delmotte, M., di Sarra, A., Sferlazzo, D.,
933 di Iorio, T., Piacentini, S., Cristofanelli, P., Mihalopoulos, N., Kouvarakis, G., Pikridas, M., Savvides, C.,
934 Mamouri, R.-E., Nisantzi, A., Hadjimitsis, D., Attié, J.-L., Ferré, H., Kangah, Y., Jaidan, N., Guth, J., Jacquet, P.,
935 Chevrier, S., Robert, C., Bourdon, A., Bourdinot, J.-F., Etienne, J.-C., Krysztofiak, G., and Théron, P.: The GLAM
936 airborne campaign across the Mediterranean basin, *Bull. Am. Met. Soc.*, 99, 361–380,
937 <https://doi.org/10.1175/BAMS-D-16-0226.1>,2018.

938 Salvador, P., Alonso-Pérez, S., Pey, J., Artíñano, B., de Bustos, J. J., Alastuey, A., and Querol, X.: African dust
939 outbreaks over the western Mediterranean Basin: 11-year characterization of atmospheric circulation patterns and
940 dust source areas, *Atmos. Chem. Phys.*, 14, 6759–6775, <https://doi.org/10.5194/acp-14-6759-2014>, 2014.

941 Shaheen, A., Wu, R., Aldabash, M., Long-term AOD trend assessment over the Eastern Mediterranean region: A
942 comparative study including a new merged aerosol product, *Atmosph. Environ.*, 238, 117736,
943 <https://doi.org/10.1016/j.atmosenv.2020.117736>,2020.

944 Sič, B., El Amraoui, L., Piacentini, A., Marécal, V., Emili, E., Cariolle, D., Prather, M., and Attié, J.-L.: Aerosol
945 data assimilation in the chemical-transport model MOCAGE during the TRAQA/ChArMEx campaign: Aerosol
946 optical depth, *Atmos. Meas. Tech.*, 9, 5535–5554, <https://doi.org/10.5194/amt-9-5535-2016>, 2016.

947 Sicard, M., R. Barragan, F. Dulac, L. Alados-Arboledas, and M. Mallet : Aerosol optical, microphysical and
948 radiative properties at regional background insular sites in the western Mediterranean, *Atmos. Chem. Phys.*, 16,
949 12177–12203,<https://doi.org/10.5194/acp-16-12177-2016>,2016.

950 Tanré, D., Bréon, F. M., Deuzé, J. L., Dubovik, O., Ducos, F., François, P., Goloub, P., Herman, M., Lifermann,
951 A. and Waquet, F.: Remote sensing of aerosols by using polarized, directional and spectral measurements within
952 the A-Train: the PARASOL mission, *Atmos. Meas. Tech.*, 4, 1383–1395, [https://doi.org/10.5194/amt-4-1383-](https://doi.org/10.5194/amt-4-1383-2011)
953 [2011](https://doi.org/10.5194/amt-4-1383-2011), 2011.

954

955

956

957

958

959

960

961

962

963

964

965
966
967
968
969
970
971
972
973
974
975
976
977
978
979
980
981
982

	AOD			AE			AOD _F			AOD _c		
	North	Central	South	North	Central	South	North	Central	South	North	Central	South
Winter (DJF)	0.062	0.064	0.074	0.950	0.792	0.723	0.025	0.022	0.021	0.037	0.042	0.058
Spring (MAM)	0.106	0.115	0.155	1.064	0.855	0.724	0.043	0.038	0.040	0.063	0.078	0.115
Summer (JJA)	0.106	0.126	0.153	0.947	0.819	0.737	0.038	0.038	0.040	0.068	0.088	0.113
Fall (SON)	0.079	0.086	0.104	0.963	0.831	0.734	0.033	0.030	0.031	0.047	0.057	0.074
Annual	0.090	0.099	0.124	0.985	0.826	0.729	0.035	0.032	0.033	0.055	0.067	0.091
	Fine Mode Fraction %			AOD _{CNS}			AOD _{CS}					
	North	Central	South	North	Central	South	North	Central	South			
Winter (DJF)	40	34	30	0.033	0.034	0.048	0.013	0.016	0.018			
Spring (MAM)	42	34	29	0.048	0.062	0.088	0.021	0.026	0.029			
Summer (JJA)	36	31	27	0.046	0.058	0.091	0.021	0.027	0.031			
Fall (SON)	40	35	30	0.041	0.047	0.059	0.015	0.019	0.023			
Annual	40	33	29	0.043	0.051	0.073	0.018	0.022	0.026			

983
984
985
986
987
988
989

Table 1a. The 8 (winter) or 9-year (March 2005 – October 2013) climatological seasonal averaged values of POLDER-3 advanced aerosol products at 865 nm for the north (NW MED), central (CW MED), and south (SW MED) parts of western Mediterranean basins (defined in Figure 2). Maximum values are reported in red, minimum, in blue.

	AOD			AOD _F			AOD _c			Fine Mode Fraction %		
	North	Central	South	North	Central	South	North	Central	South	North	Central	South
Winter (DJF)	0.099	0.093	0.106	0.069	0.059	0.058	0.030	0.035	0.049	65	60	56
Spring (MAM)	0.168	0.166	0.204	0.118	0.104	0.109	0.049	0.062	0.095	70	62	57
Summer (JJA)	0.163	0.180	0.208	0.110	0.110	0.117	0.053	0.070	0.091	66	61	57
Fall (SON)	0.126	0.128	0.144	0.089	0.082	0.084	0.037	0.046	0.060	66	61	57
Annual	0.141	0.143	0.167	0.098	0.089	0.093	0.043	0.053	0.074	67	61	57

990
991
992
993
994
995
996
997
998
999
1000
1001
1002

Table 1b. Same as Table 1a for AOD, AOD_F, AOD_c, and Fine Mode Fraction at 550 nm for the north (NW MED), central (CW MED), and south (SW MED) parts of western Mediterranean basins (defined in Figure 2). Maximum values are reported in red, minimum, in blue.

1003
 1004
 1005
 1006
 1007
 1008
 1009
 1010
 1011
 1012
 1013
 1014
 1015
 1016
 1017
 1018
 1019
 1020
 1021
 1022

	Ersa N _{ACSP} = 1242 - N _{BVC} = 556		Barcelona N _{ACSP} = 1241 - N _{BVC} = 540		Lampedusa N _{ACSP} = 1320 - N _{BVC} = 612	
	Mean ± SD	Range Min – Max	Mean ± SD	Range Min – Max	Mean ± SD	Range Min – Max
ACSP AOD _{865 nm}	0.09 ± 0.07	0.01 – 0.68	0.10 ± 0.04	0.01 – 1.05	0.15 ± 0.18	0.02 – 4.72
ACSP AOD _{F 865 nm}	0.03 ± 0.03	<0.01 – 0.16	0.04 ± 0.03	<0.01 – 0.19	0.04 ± 0.03	<0.01 – 0.35
ACSP AOD _{C 865 nm}	0.06 ± 0.06	<0.01 – 0.65	0.07 ± 0.07	<0.01 – 0.94	0.11 ± 0.16	<0.01 – 4.37
ACSP AE ₈₆₅₋₆₇₀	0.94 ± 0.53	0.01 – 2.23	0.90 ± 0.50	-0.07 – 2.33	0.67 ± 0.42	0.00 – 2.24
ACSP FMF (%)	38 ± 23	3 – 100	37 ± 22	1 – 97	28 ± 18	3 – 100
BVC AOD _{CNS 865nm}	0.04 ± 0.04	<0.01 – 0.48	0.05 ± 0.05	<0.01 – 0.42	0.08 ± 0.09	<0.01 – 1.00
BVC AOD _{CS 865nm}	0.02 ± 0.03	<0.01 – 0.24	0.02 ± 0.03	<0.01 – 0.34	0.03 ± 0.03	<0.01 – 0.33

1023
 1024
 1025
 1026
 1027
 1028
 1029
 1030
 1031
 1032
 1033
 1034
 1035
 1036
 1037
 1038
 1039

Table 2. Statistics of POLDER-3 daily retrievals of AOD, AOD_F, AOD_C, AE, FMF (Fine Mode Fraction), AOD_{CS}, and AOD_{CNS} at three main stations, Ersa, Barcelona, and Lampedusa for the period March 2005 - October 2013. The numbers of POLDER-3 retrievals available at each station for all clear sky pixels (ACSP) and for best viewing conditions (BVC) are reported.

1040
1041
1042
1043
1044
1045
1046
1047
1048
1049
1050
1051
1052
1053
1054
1055
1056
1057
1058
1059
1060
1061
1062

Trend per year Region	AOD 865 nm		AOD _{COARSE} 865 nm		AOD _{FINE} 865 nm	
	Annual means	Monthly anomalies	Annual means	Monthly anomalies	Annual means	Monthly anomalies
NW MED	- 0.0030 ± 0.0011*	- 0.0031 ± 0.0006**	- 0.0010 ± 0.0009	- 0.0012 ± 0.0005*	- 0.0020 ± 0.0005**	- 0.0019 ± 0.0003**
CW MED	- 0.0035 ± 0.0010*	- 0.0035 ± 0.0007**	- 0.0015 ± 0.0009	- 0.0016 ± 0.0006**	- 0.0020 ± 0.0004**	- 0.0019 ± 0.0003**
SW MED	- 0.0037 ± 0.0019	- 0.0043 ± 0.0012**	- 0.0021 ± 0.0016	- 0.0027 ± 0.0010*	- 0.0016 ± 0.0004**	- 0.0016 ± 0.0003**

1063
1064
1065
1066
1067
1068
1069
1070
1071

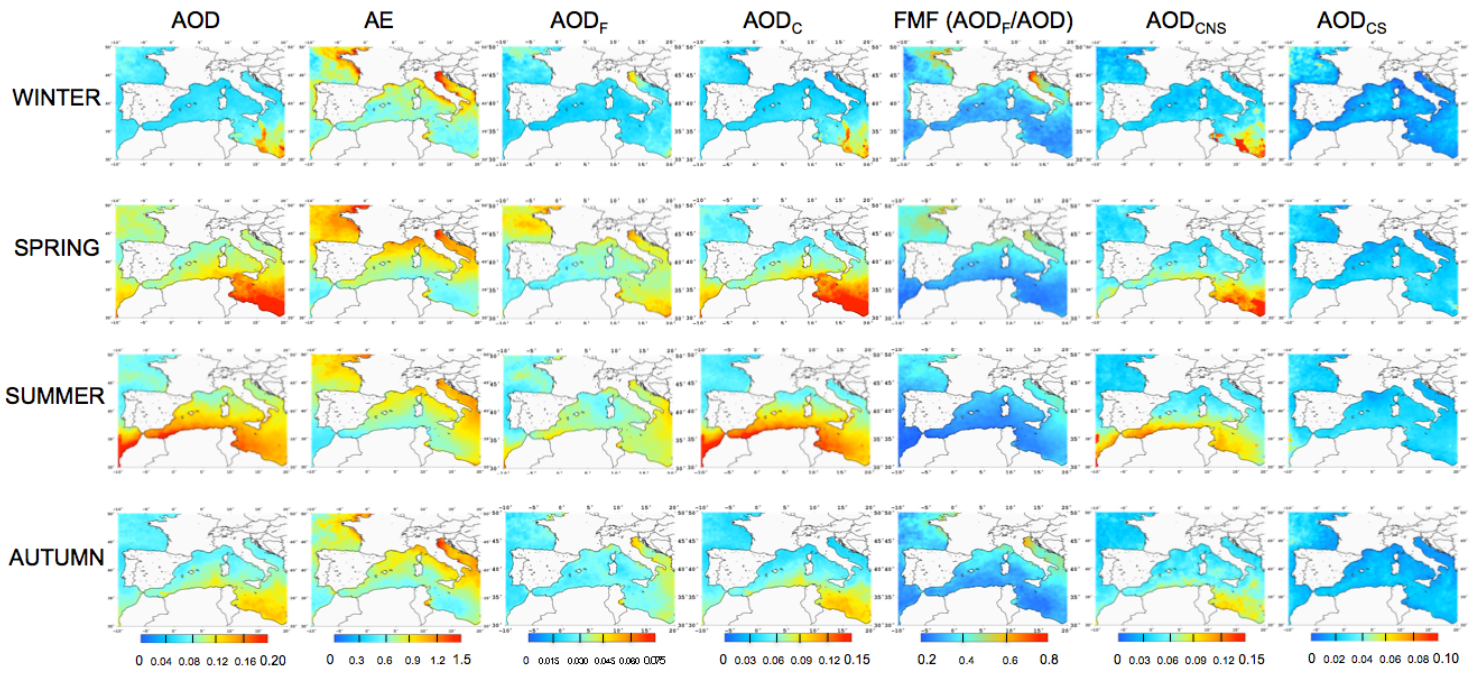
Table 3. POLDER-3 865 nm AOD, AOD_{COARSE} and AOD_{FINE} trends per year derived from March-October annual means and monthly mean anomalies over the 2005-2013 period for NW MED, CW MED, SW MED. The corresponding annual evolutions are shown in Figure 89 and S6 (left columns). Trends (year⁻¹) are shown with their standard deviations (± 1σ). Values in bold indicate statistically significant trends at * 95% confidence level and ** 99% confidence level, as determined by the Student t-test.

Trend per year Station	AOD 865 nm		AOD _{COARSE} 865 nm		AOD _{FINE} 865 nm	
	Annual means	Monthly anomalies	Annual means	Monthly anomalies	Annual means	Monthly anomalies
Ersa	- 0.0035 ± 0.0014*	- 0.0030 ± 0.0008**	- 0.0012 ± 0.0012	- 0.0011 ± 0.0008	- 0.0024 ± 0.0004**	- 0.0019 ± 0.0003**
Barcelona	- 0.0050 ± 0.0021*	- 0.0046 ± 0.0011**	- 0.0021 ± 0.0017	- 0.0020 ± 0.0009*	- 0.0029 ± 0.0005**	- 0.0026 ± 0.0004**
Lampedusa	- 0.0037 ± 0.0028	- 0.0025 ± 0.0018	- 0.0021 ± 0.0026	- 0.0009 ± 0.0016	- 0.0017 ± 0.0003**	- 0.0015 ± 0.0004**

1072
1073
1074
1075
1076
1077
1078
1079
1080

Table 4. POLDER-3 865 nm AOD, AOD_{COARSE} and AOD_{FINE} trends per year derived from March-October annual means and monthly mean anomalies over the 2005-2013 period for Ersa, Barcelona, and Lampedusa. The corresponding annual evolutions are shown in Figure 9 and S6 (right columns). Trends (year⁻¹) are shown with their standard deviations (± 1σ). Values in bold indicate statistically significant trends at * 95% confidence level and ** 99% confidence level, as determined by the Student t-test.

1081
1082



1083
1084

Figure 1. Climatological seasonal maps for AOD, AE, AOD_F, AOD_C, FMF (Fine Mode Fraction derived from AOD_F/AOD), AOD_{CNS}, and AOD_{CS} retrieved by POLDER-3 at 865 nm over the period March 2005-October 2013. Seasons are ordered from the top to the bottom : Winter is December-January-February, Spring March-April-May, Summer June-July-August, Autumn September-October-November.

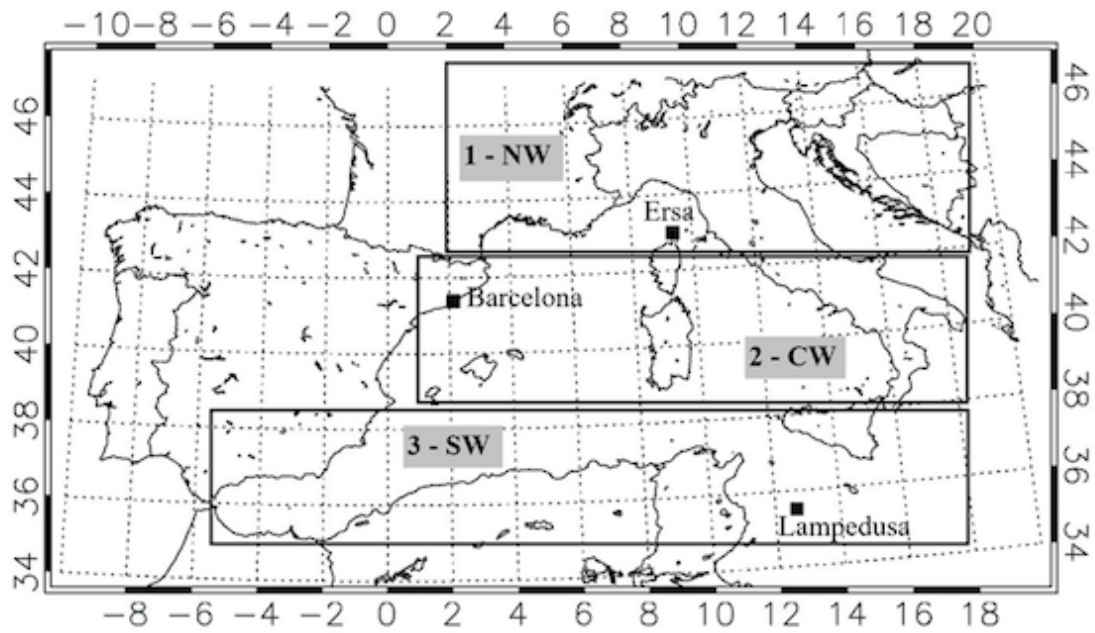


Figure 2. Definition of the three geographical sub-regions used to analyze POLDER-3 aerosol retrievals over the area of study: 1. NW Med, 42-46°N, 02°E-20°E – 2. CW MED, 38-42°N, 01°W-20°E, 3. SW MED, 34-38°N, 06°W-20°E. The three sites considered in this study are reported, i.e., Ersat (43.00367°N, 09.35929°E), Barcelona (41.38925°N, 02.11206°E), and Lampedusa (35.51667°N, 12.63167°E).

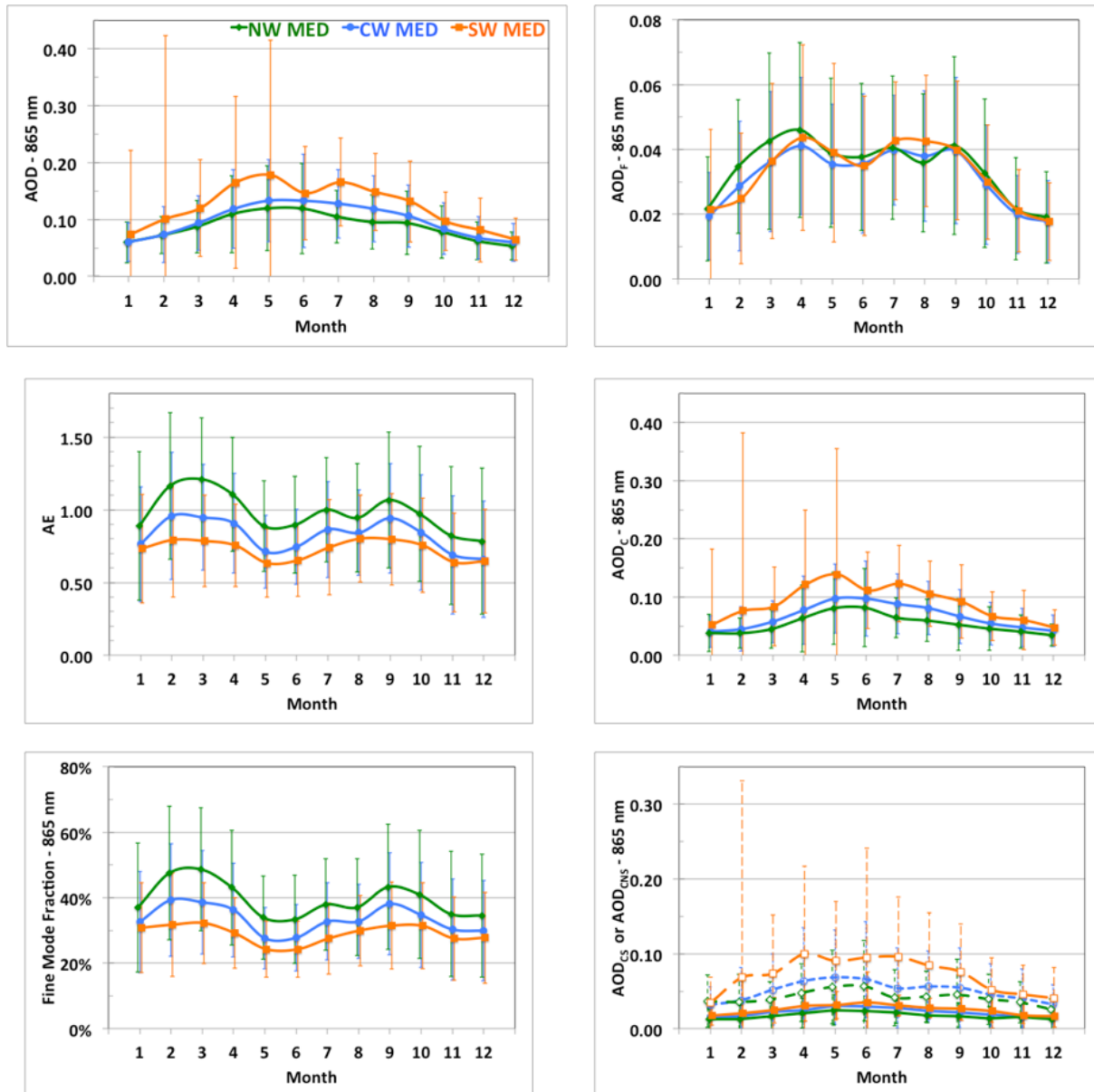


Figure 3. The 9-year (March 2005 – October 2013) climatological seasonal cycle of -Left column: AOD (top), Angström Exponent (middle), Fine Mode Fraction (bottom) – Right column: AOD_{Fine} (top), AOD_{Coarse} (middle), AOD_{Coarse Spherical} (continuous lines) and AOD_{Coarse Non Spherical} (dashed lines) (bottom), derived from POLDER-3 at 865 nm. The green, blue, orange curves are respectively for the north (NW MED), central (CW MED), and south (SW MED) parts of western Mediterranean basins (defined in Figure 2).

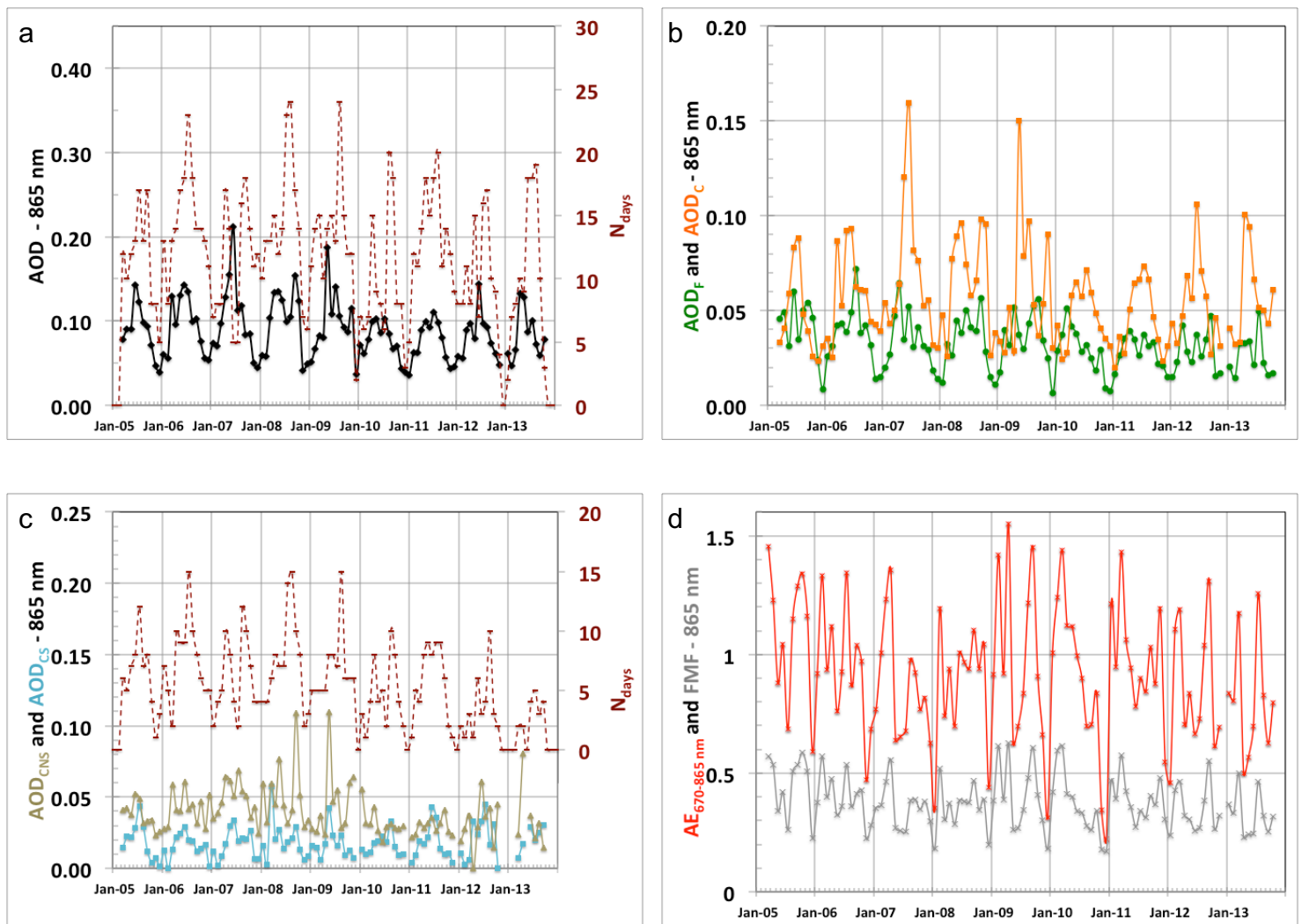


Figure 4. POLDER-3 monthly mean retrievals of (a) AOD, (b) AOD_F and AOD_C , (c) AOD_{CNS} and AOD_{CS} , (d) $AE_{865-670}$ and FMF at 865 nm at Ersa over the period 2005-2013. The number of days of observations available for each month is reported for all clear days (right axis of Figure 4a), and for best viewing conditions (right axis of Figure 4c) necessary for retrievals of AOD_{CNS} and AOD_{CS} .

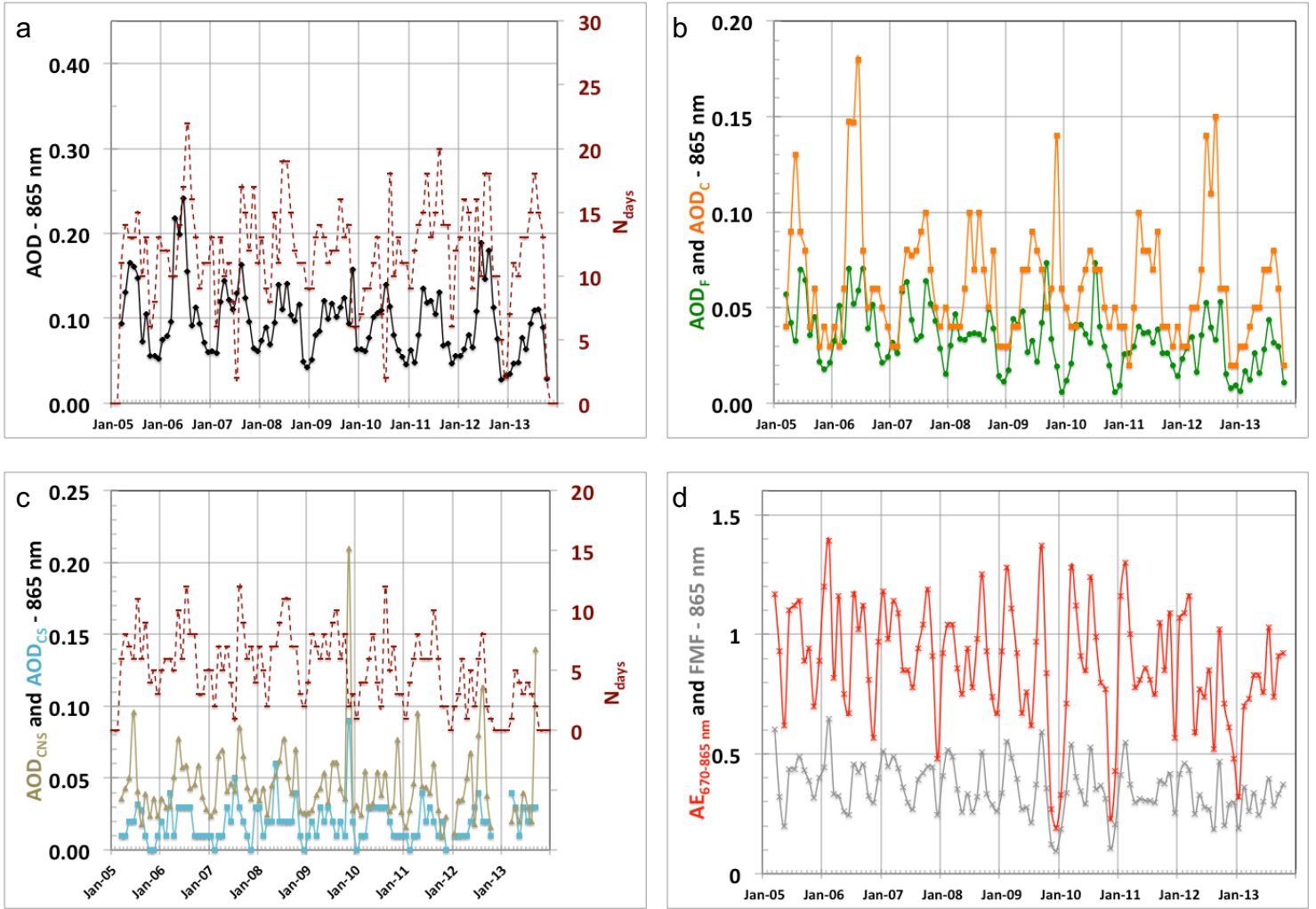


Figure 5. Same as Figure 4 for Barcelona.

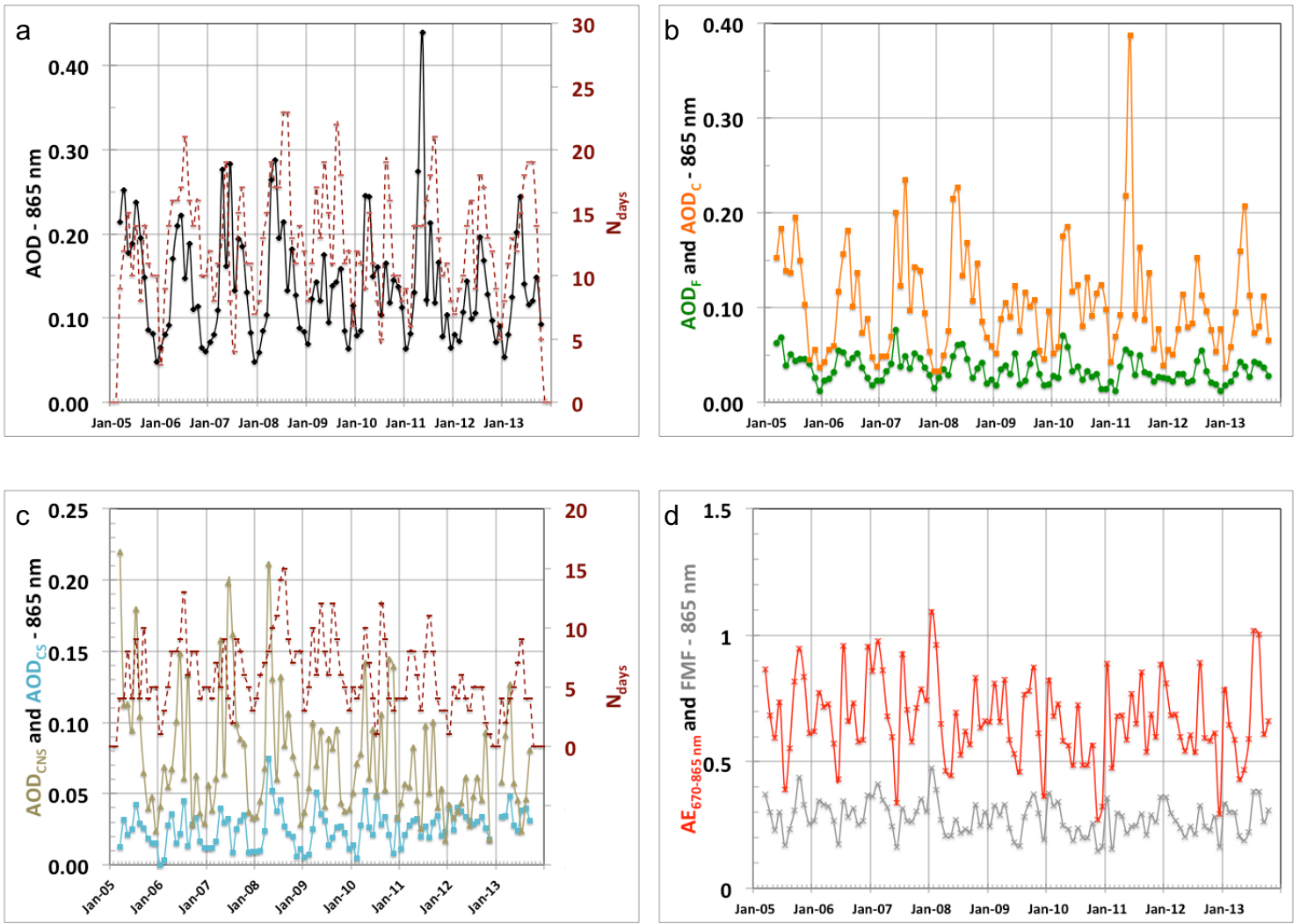


Figure 6. Same as Figure 4 for Lampedusa. Note that the scale of Figure 6b is different from that of Figure 4b and 5b.

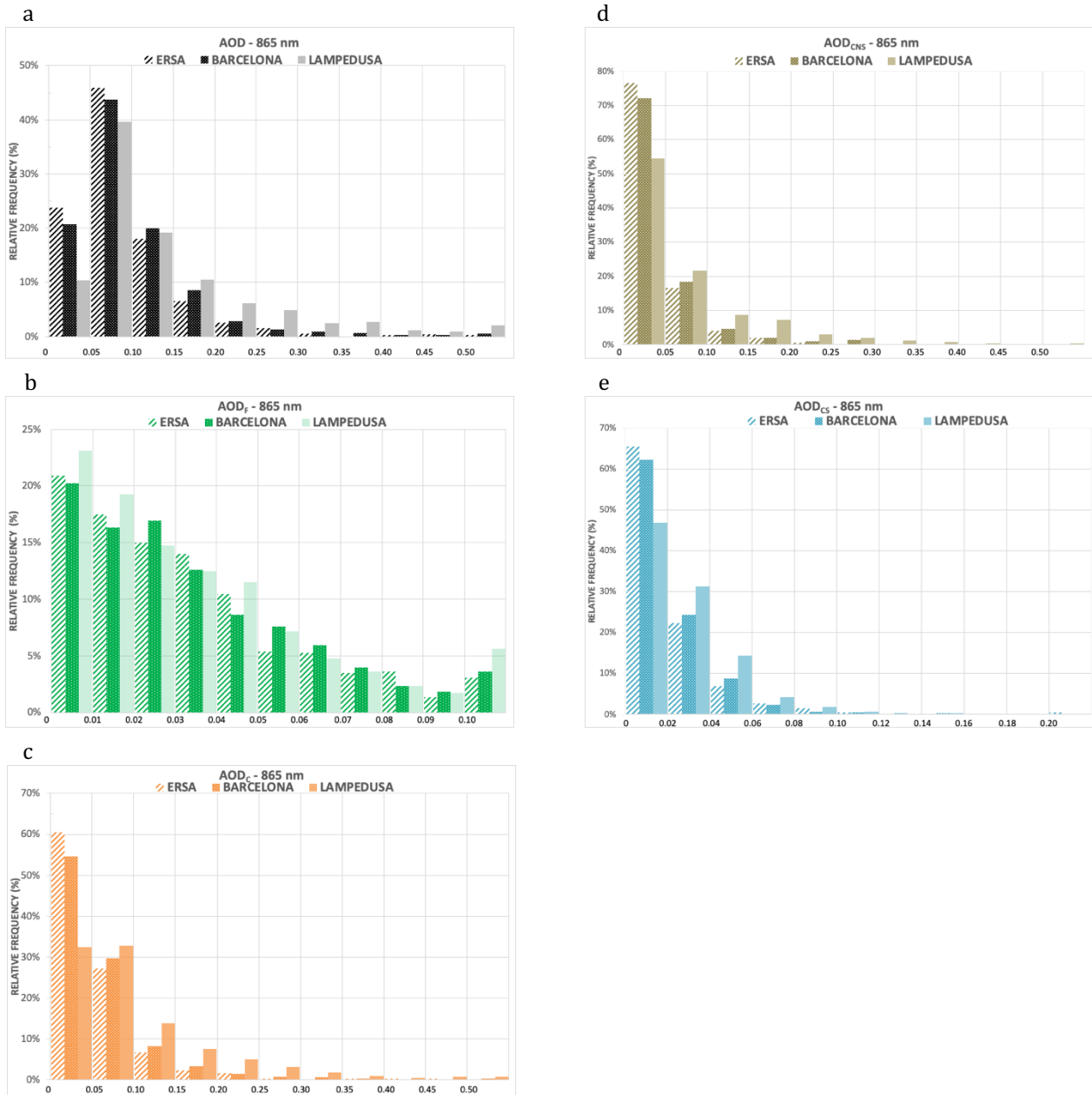


Figure 7. POLDER-3 daily retrievals of a- AOD, b- AOD_F, c- AOD_C, d- AOD_{CNS} and AOD_{CS} at 865 nm at Ersa (left panels), Barcelona (middle panels), and Lampedusa (right panels) over its whole period of operation (March 4, 2005—October 10, 2013). Frequency histograms for POLDER-3 daily retrievals at 865 nm of a- AOD, b- AOD_F, c- AOD_C, d- AOD_{CNS}, e- AOD_{CS} at Ersa, Barcelona, and Lampedusa.

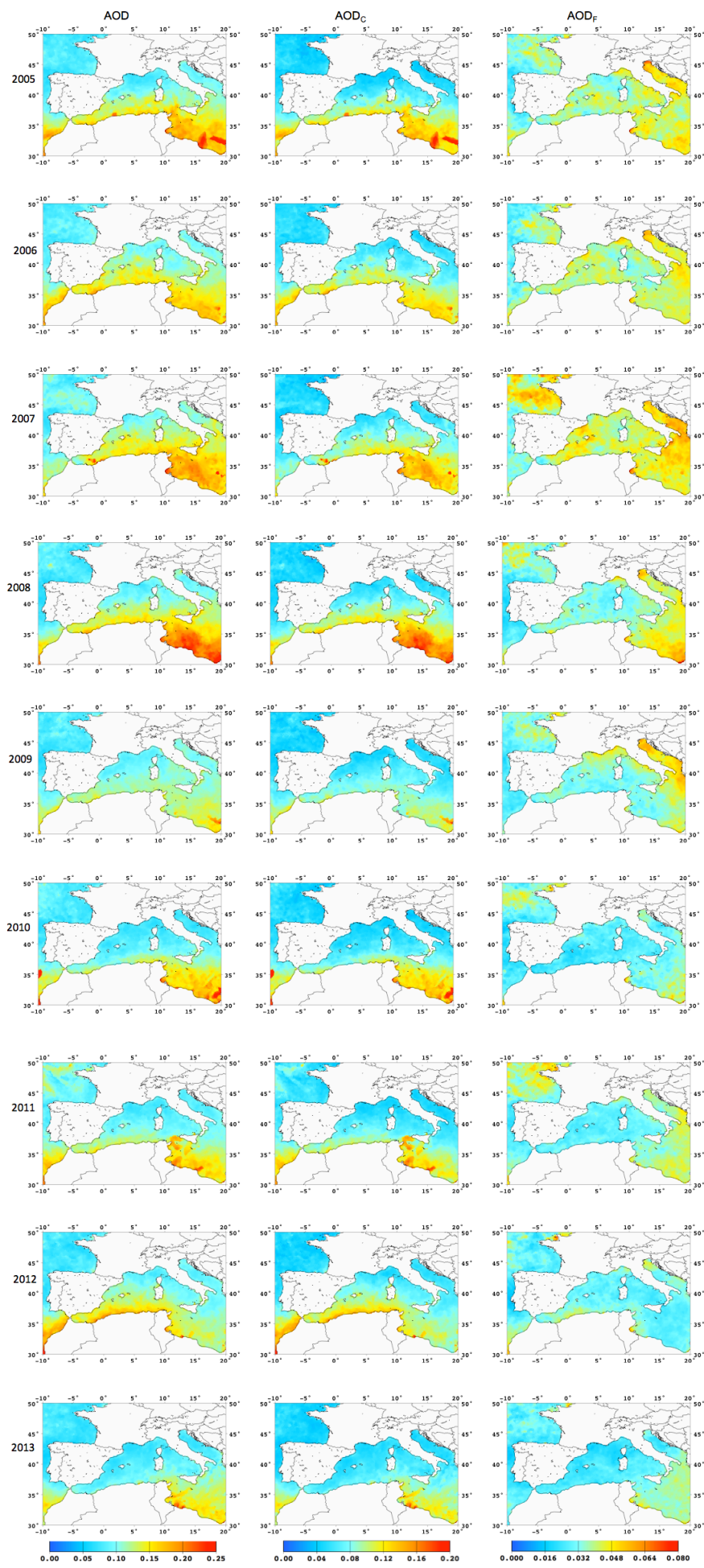


Figure 8. March-October annual averages of POLDER-3 AOD (left), AOD_C (middle), AOD_F (right) at 865 nm from 2005 to 2013.

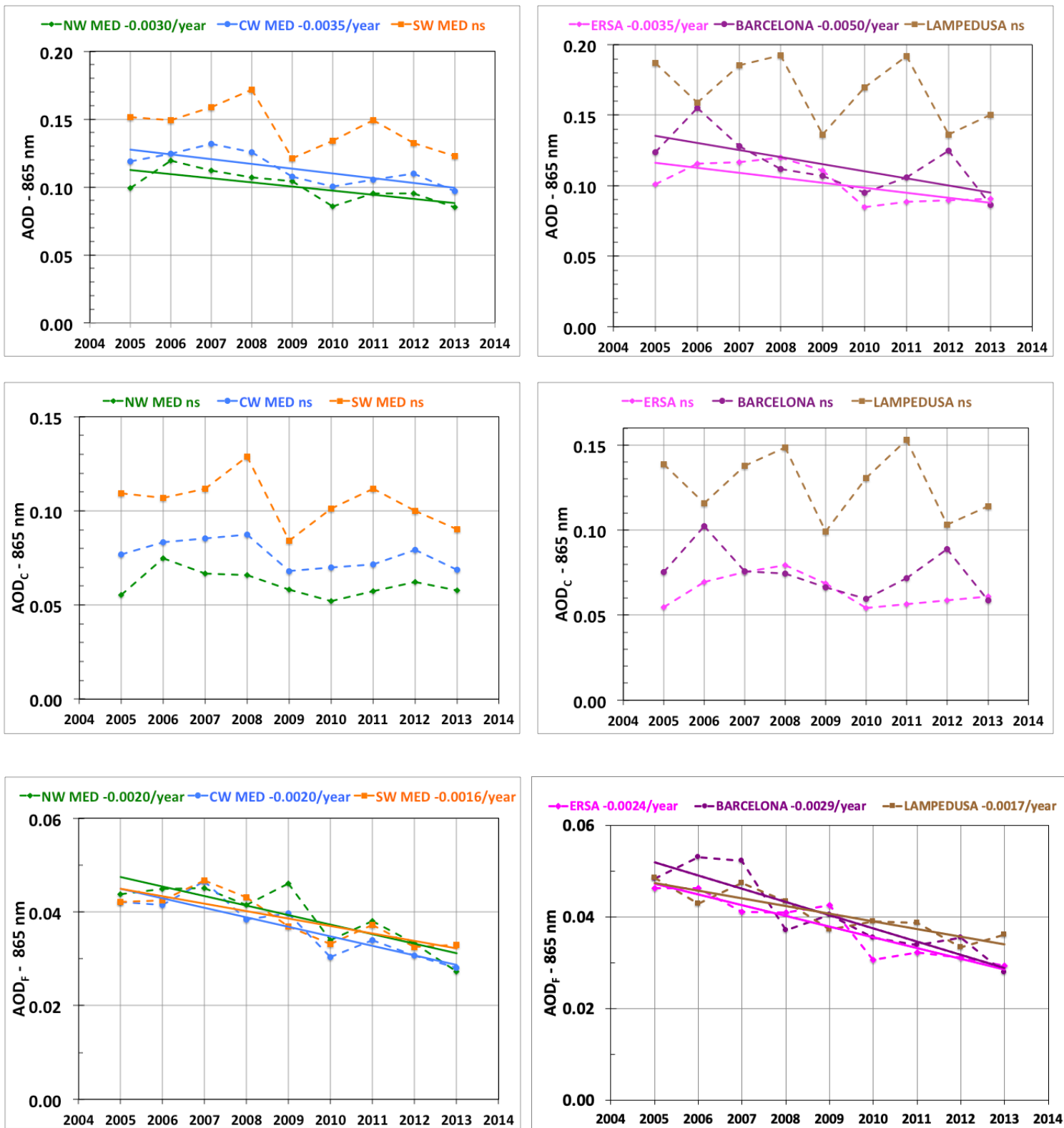


Figure 9. March to October yearly means (left column) and monthly anomalies (right column) of POLDER-3 retrievals at 865 nm over the period 2005–2013: AOD (top), AOD_{COARSE} (middle), AOD_{FINE} (bottom). In the left column, spatially averaged values over north (NW MED, green curves), central (CW MED, blue curves), and south (SW MED, orange curves) parts of western Mediterranean basins (defined Figure 2). In the right column, values extracted at Ersar (pink curves), Barcelona (purple curves), and Lampedusa (brown curves). Trends (year⁻¹) are plotted when significant according to the Student t-test, as summarized in Table 3.

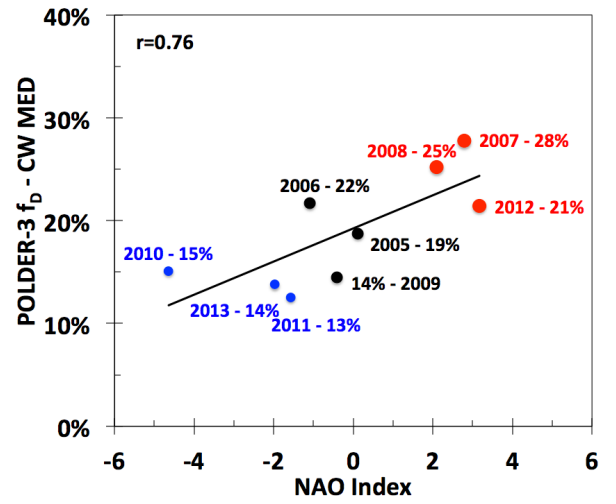
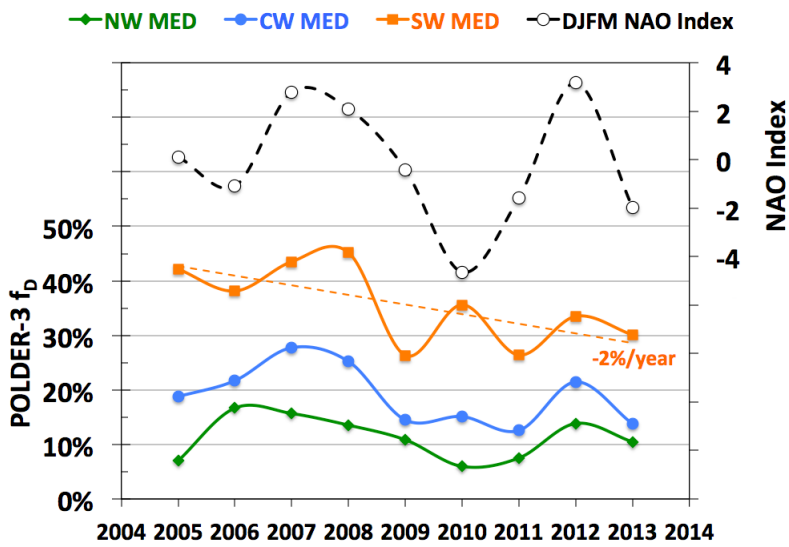


Figure 11.10 Left: Time series of the NAO winter Index (scale on the right axis, open circles) and of the following annual relative frequency (f_D) of POLDER-3 AOD_c at 865 nm ≥ 0.10 for the three sub-regions (NW MED in green, CW MED in blue, SW MED in orange) over the period March-2005–October 2013. The only significant trend of f_D /year is reported on the graph for SW MED. Right: Scatterplot of f_D versus preceding winter NAO Index for the CW MED region.

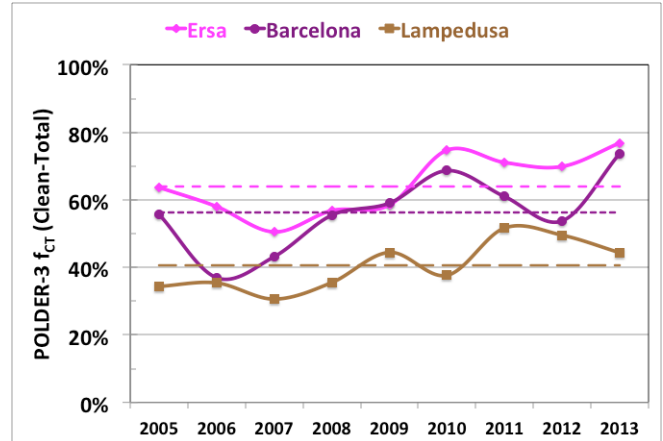
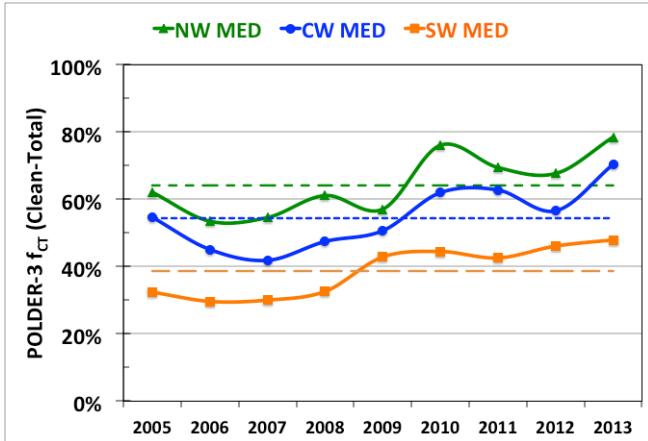
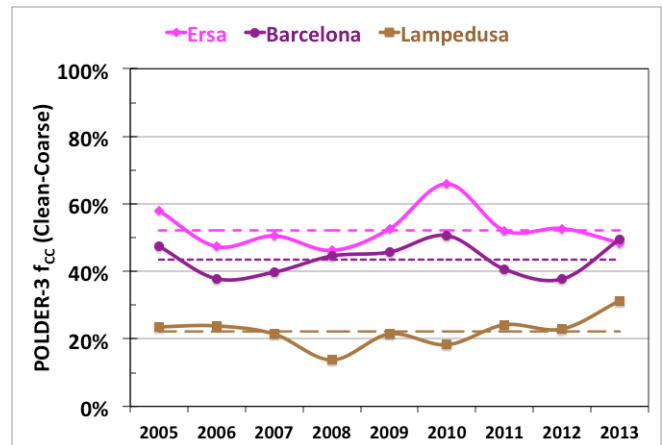
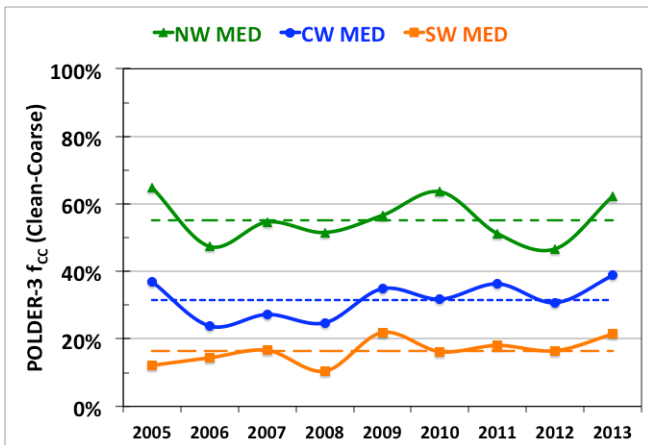
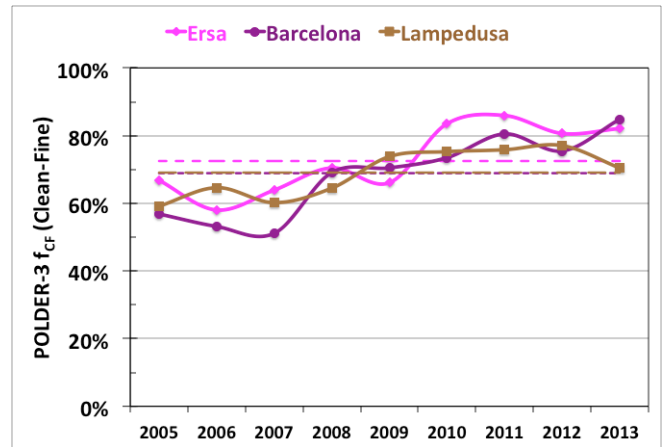
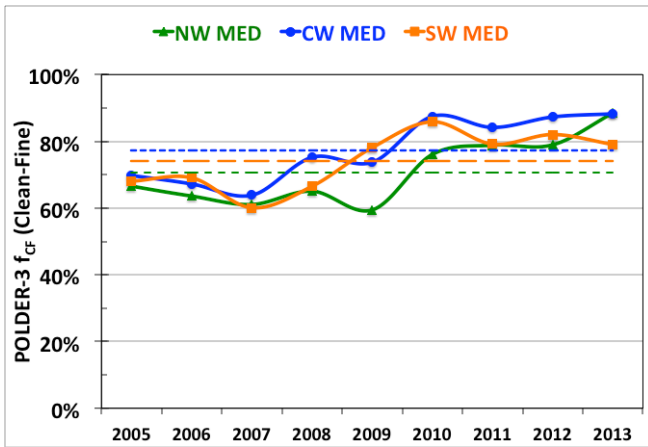


Figure 1211. Left: Time series of annual (March–October) relative frequencies of occurrence of clean conditions for fine mode aerosol component (POLDER-3 AOD_F 865 nm below 0.05, f_{CF} ; top panel), coarse mode aerosol component (POLDER-3 AOD_C 865 nm below 0.05, f_{CC} ; middle panel), and total aerosol (POLDER-3 AOD 865 nm lower or equal to 0.10, f_{CT} ; bottom panel) over the period 2005–2013 for the three sub-regions NW MED, CW MED, SW MED. The dashed lines indicate the multi-year annual averages of relative frequencies. Right: Same for the three sites of Ersa, Barcelona, and Lampedusa.

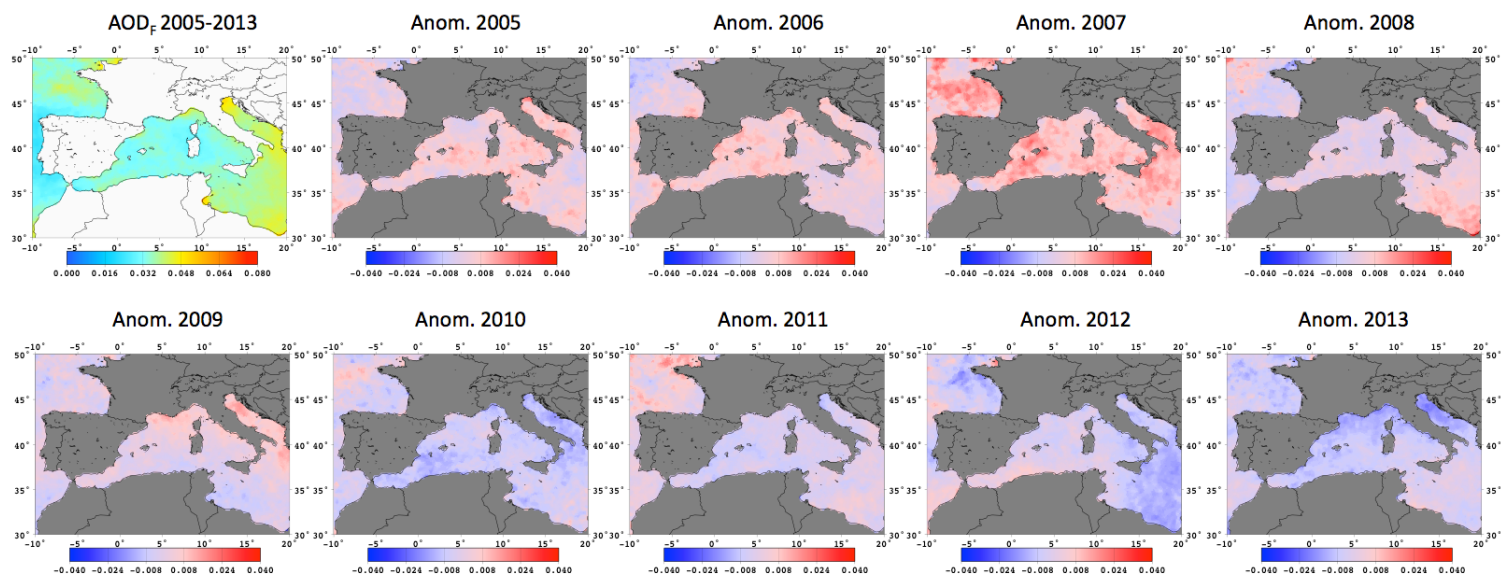


Figure 1312. POLDER-3 AOD_F at 865 nm averaged over the March-October period and the 9 years 2005-2013 (top left) and associated AOD_F anomalies for each year.

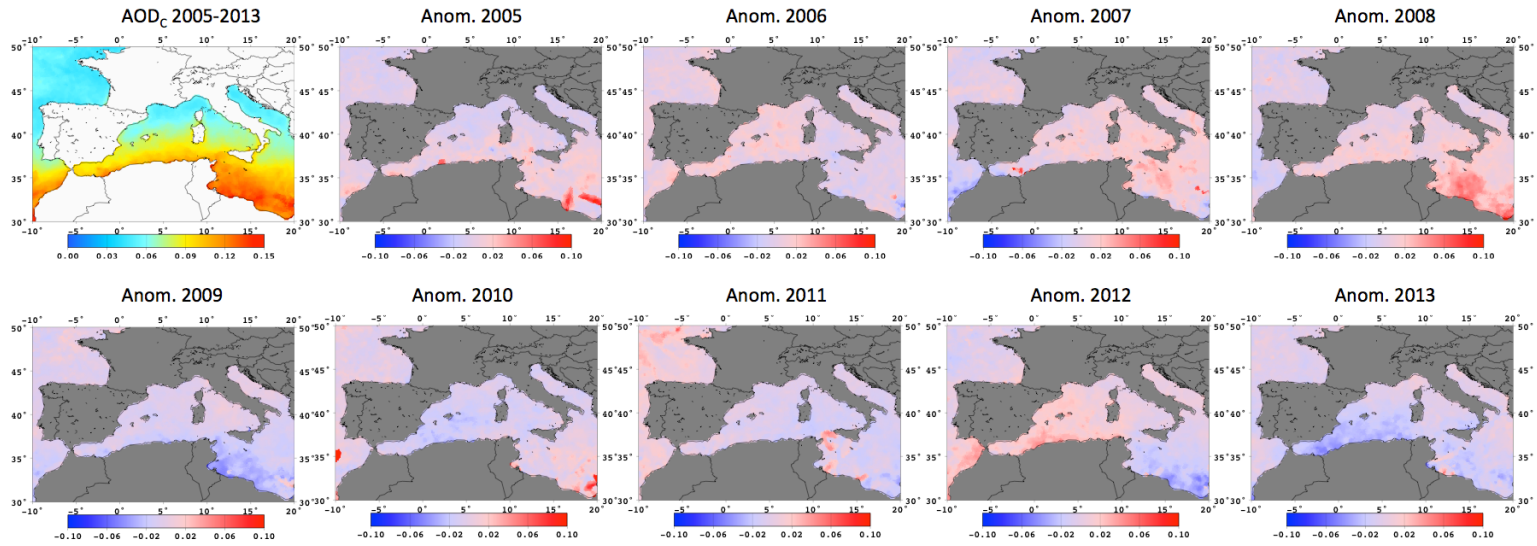


Figure 1413. POLDER-3 AOD_C at 865 nm averaged over the March-October period and the 9 years 2005-2013 (top left) and associated AOD_C anomalies for each year.